The Schistosoma mansoni tegumental allergen protein, SmTAL1: binding to an IQ-motif from a voltage-gated ion channel and effects of praziquantel.

Calmodulins from *Schistosoma mansoni*: biochemical analysis and interaction with IQ-motifs from voltage-gated calcium channels

Charlotte M. Thomas and David J. Timson

- *S. mansoni* has two calmodulins with very similar biochemical properties
- Both proteins interact with Ca^{2+}, Mn^{2+}, Cd^{2+}, Fe^{2+} and Pb^{2+} ions
- Both interact with an IQ-motif from the voltage-gated calcium channel $SmCa_V1B$
- The affinity of this interaction is slightly increased by calcium ions
- Chlorpromazine and trifluoperazine antagonise these interactions

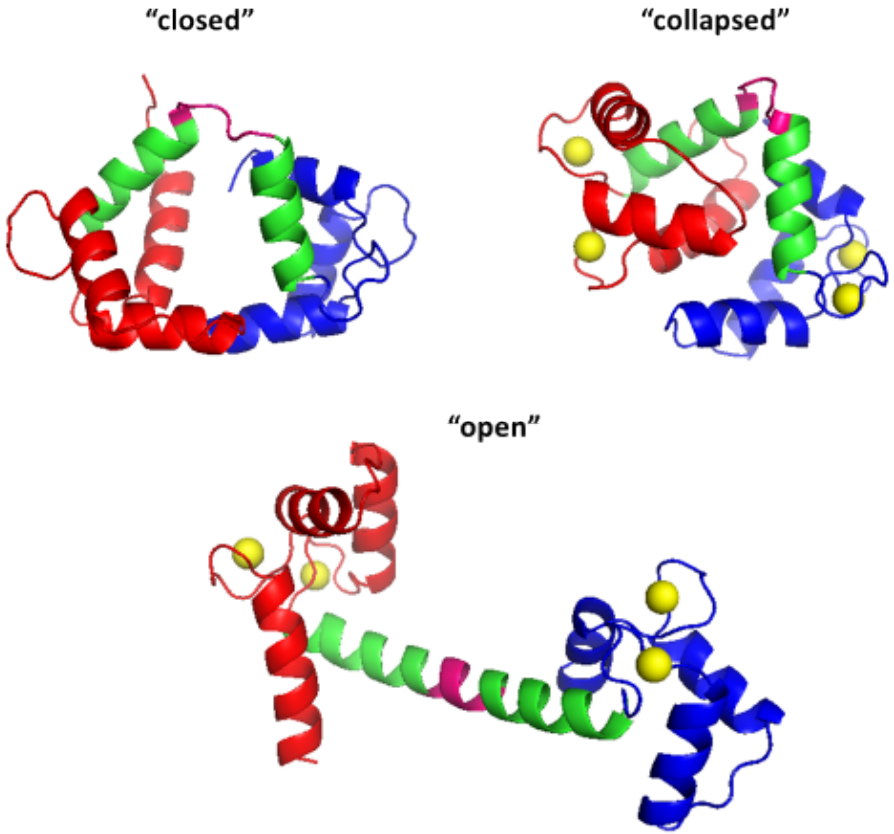
"closed"
"collapsed"
"open"

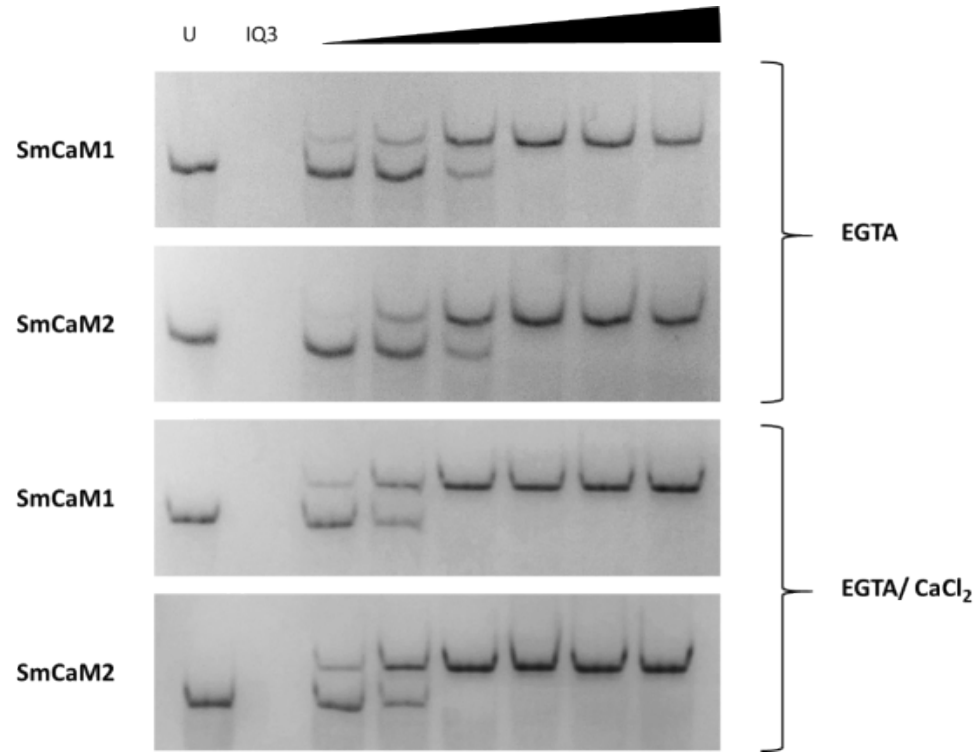
U
IQ3
SmCaM1
SmCaM2
SmCaM1
SmCaM2
EGTA
EGTA/ CaCl2

Calmodulins from *Schistosoma mansoni*: biochemical analysis and interaction with IQ-motifs from voltage-gated calcium channels

Charlotte M. Thomas[1] and David J. Timson[1,2]*

[1] School of Biological Sciences, Queen's University Belfast, Medical Biology Centre, 97 Lisburn Road, Belfast, BT9 7BL, UK and Institute for Global Food Security, Queen's University Belfast, 18-30 Malone Road, Belfast, BT9 5BN, UK.

[2] School of Pharmacy and Biomolecular Sciences, University of Brighton, Huxley Building, Lewes Road, Brighton, BN2 4GJ. UK.

*Author to whom correspondence should be addressed at School of Pharmacy and Biomolecular Sciences, University of Brighton, Huxley Building, Lewes Road, Brighton, BN2 4GJ. UK.

Telephone +44(0)1273 641623

Fax +44(0)1273 642090

Email d.timson@brighton.ac.uk

Running title: *S. mansoni* calmodulins

Abstract

The trematode *Schistosoma mansoni* is a causative agent of schistosomiasis, the second most common parasitic disease of humans after malaria. Calcium homeostasis and calcium-mediated signalling pathways are of particular interest in this species. The drug of choice for treating schistosomiasis, praziquantel, disrupts the regulation of calcium uptake and there is interest in exploiting calcium-mediated processes for future drug discovery. Calmodulin is a calcium sensing protein, present in most eukaryotes. It is a critical regulator of processes as diverse as muscle contraction, cell division and, partly through interaction with voltage-gated calcium channels, intra-cellular calcium concentrations. *S. mansoni* expresses two highly similar calmodulins – SmCaM1 and SmCaM2. Both proteins interact with calcium, manganese, cadmium (II), iron (II) and lead ions in native gel electrophoresis. These ions also cause conformational changes in the proteins resulting in the exposure of a more hydrophobic surface (as demonstrated by anilinonaphthalene-8-sulfonate fluorescence assays). The proteins are primarily dimeric in the absence of calcium ions, but monomeric in the presence of this ion. Both SmCaM1 and SmCaM2 interact with a peptide corresponding to an IQ-motif derived from the α-subunit of the voltage-gated calcium channel $SmCa_v1B$ (residues 1923-1945). Both proteins bound with slightly higher affinity in the presence of calcium ions. However, there was no difference between the affinities of the two proteins for the peptide. This interaction could be antagonised by chlorpromazine and trifluoperazine, but not praziquantel or thiamylal. Interestingly no interaction could be detected with the other three IQ-motifs identified in *S. mansoni* voltage-gated ion calcium channels.

Keywords: calcium binding protein; calmodulin antagonist; voltage-gated calcium channel; blood fluke; neglected tropical disease

Abbreviations

ANS, anilinonaphthalene-8-sulfonate

BS^3, *bis*(sulfosuccinimidyl)suberate

CPZ, chlorpromazine

PZQ, praziquantel

rmsd, root mean square deviation

SmCaM1, one of the two calmodulins from *S. mansoni*

SmCaM2, one of the two calmodulins from *S. mansoni*

TFP, trifluoperazine

ThA, thiamylal

W7, N-(6-Aminohexyl)-5-chloro-1-naphthalenesulfonamide hydrochloride

Introduction

Calmodulin is a small (~17 kDa) calcium sensor protein which is found in almost all eukaryotes. It is known to function in calcium signalling in a wide range of distinct cellular processes including muscle contraction, calcium homeostasis and inflammation [1]. Structurally, it consists of two globular heads, linked by an extended α-helix [2, 3]. Within each globular head are two EF-hand motifs which are capable of binding calcium and other divalent cations. The EF-hand is a compact structure in which the polypeptide backbone turns tightly, creating a space for divalent cation binding in which carbonyl and carboxylate ligands point inwards to coordinate the ion [4, 5]. On binding calcium ions, calmodulin undergoes a conformational change in which the protein's surface becomes more hydrophobic [6-8]. This facilitates interaction with a range of target molecules [9, 10]. Typically, the linker helix partially "melts" enabling the two heads to move closer together and for the protein to wholly or partially wrap around extended target sequences.

One key target motif is the IQ-motif. This has the consensus sequence IQxxxRGxxxR; however considerable variation on this sequence is possible. The motif is found in proteins as diverse as myosin superfamily members, the cytoskeleton regulating IQGAP family proteins and voltage-gated ion channels. The effect of calcium ions on calmodulin-IQ-motif interactions varies. In some cases, the interaction requires calcium ions whereas others are promoted in the absence of calcium and some are independent of calcium concentrations [11-13]. Structurally, the IQ-motif typically forms an extended α-helix which calmodulin (and structurally similar proteins such as myosin light chains) can wrap around [14-17].

Voltage-gated calcium channels (Ca_v channels) regulate the influx of calcium into cells. These channels are multimeric protein complexes consisting of a large, pore-forming Ca_v α_1 subunit, attached to two smaller auxiliary subunits, termed Ca_v β and Ca_v $\alpha_2\delta$ [18]. The cytoplasmic β subunit

acts to modulate the activity of the channel whilst directing expression to the plasma membrane [19], whereas the heterodimeric $\alpha_2\delta$ subunit acts as a transmembrane receptor for various anti-epileptic drugs [20]. Although both auxiliary subunits play important regulatory roles in the protein complex, it is the α_1 subunit that primarily defines the pharmacological and functional profile of the channel. Ca_v α_1 subunits are defined by the type of current they gate, and can be distinguished by various kinetic parameters or pharmacological characteristics [18]. For example, long-lasting, L-type Ca_v channels have a high voltage of activation (HVA), and a slow inactivation rate [18]. These channels are formed by Ca_v1-type α_1 subunits (including the $Ca_v1.1$, $Ca_v1.2$, $Ca_v1.3$ and $Ca_v1.4$ sub-families) and are further characterised by their sensitivity to various antagonistic drugs, most notably those of the dihydropyridine (DHP) class [21-23]. Mammals typically express a complement of ten Ca_v α_1 subunits, whereas invertebrate species tend to contain a single representative from each Ca_v1, Ca_v2 and Ca_v3 subtypes [18, 24]. However, these trends do not apply to members of the *Schistosoma* genus [25]. Initial work revealed the existence of three *Schistosoma mansoni* voltage-gated calcium channels ($SmCa_v$), designated $SmCa_v1A$, $SmCa_v2A$ and $SmCa_v2B$ [26]. Subsequent annotation of the *S. mansoni* genome indicated the existence of a fourth, designated $SmCa_v1B$ [27]. Furthermore, as $SmCa_v1$ α_1 subunits ($SmCa_v1A$ and $SmCa_v1B$) share highest sequence identity with vertebrate Ca_v1 (L-type) channels, whereas $SmCa_v2$ isotypes ($SmCa_v2A$ and $SmCa_v2B$) share highest sequence identity with Ca_v2 (P/Q, N and R-type) channels, this suggests that schistosomes encode four HVA channels, yet possess no equivalent to the LVA (T-type) channel [25].

Depending on local or global calcium ion concentrations, Ca^{2+}-CaM binding at the C-terminal region of the Ca_v α_1 subunit can either attenuate the influx of calcium ions through the channel pore, in a process called calcium-dependent inactivation (CDI), or it can promote calcium influx, in a process called calcium-dependent facilitation (CDF) [28-32]. Furthermore, the C-terminal region of the α_1 subunit is believed to function as a binding site for apo-CaM, allowing constitutive tethering of the

calcium sensor [28, 33, 34].

Schistosomiasis (bilharzia) is a parasitic disease which results from infections by worms from the genus *Schistosoma*. It is second only to malaria in terms of the number of humans affected by parasitic infections and the majority of cases are in the developing world [35]. In schistosomes (and some other helminth parasites) disruption of calcium homeostasis is one consequence of the administration of the anthelminthic drug praziquantel (PZQ) [36-42]. A number of authors have hypothesised that PZQ acts by disruption of voltage-gated calcium channels; however, the molecular details of this have yet to be discovered [38, 39]. Nevertheless, this suggests that calcium signalling molecules are worthy of further study as potential targets for novel anti-schistosomal drugs. It has been shown previously that *Schistosoma mansoni* has two calmodulin isotypes. These two isotypes are highly similar, differing only by two amino acid residues towards the C-termini [43]. Despite this high level of similarity the available evidence suggests that the proteins are derived from separate genes [43]. The calmodulin antagonist trifluoperazine (TFP) reduced miracidium-to-sporocyst transformation in a dose-dependent manner suggesting a critical involvement for one or both calmodulin isotypes in this process [43]. This compound has also been shown to collapse the tegumental membrane potential and to disrupt the ultrastructure of the tegument [44]. Earlier work demonstrated that calmodulin is also required for egg hatching in *S. mansoni* [45]. Here, we present the biochemical characterisation of the two known calmodulin isotypes from *S. mansoni* including the identification of a likely binding site in one of the parasite's voltage-gated calcium channels.

Materials and Methods

Molecular modelling

Initial molecular models of SmCaM1 and SmCaM2 in the "closed" conformation were generated

using Phyre2 in the intensive mode [46, 47]. These were energy minimised using YASARA (http://www.yasara.org) [48]. To generate calcium-bound forms of the two proteins, the minimised models were aligned (using PyMol, www.pymol.org) with the most similar structure identified by Phyre2 (potato calmodulin, 1RFJ [49]). New models were generated by saving either SmCaM1 or SmCaM2 with the calcium ions from 1RFJ. To generate the final, calcium-bound structures, these models were then minimised with YASARA. The templates for the remaining *S. mansoni* calmodulin (SmCaM1 and SmCaM2) homology models were: Ca^{2+}-CaM in the "open" conformation, *Rattus rattus* calmodulin (PDB: 3CLN) [50]; Ca^{2+}-CaM in the "collapsed" conformation, *Bos taurus* calmodulin (PDB: 1PRW) [51]; Apo-CaM in the homodimeric state, *Rattus norvegicus* calmodulin (PDB: 1QX5) [52]; Ca^{2+}-CaM-IQ peptide complex, *Homo sapiens* calmodulin in complex with an IQ peptide derived from the human $Ca_v1.2$ channel α_1 subunit, $HsCa_v1.2$ (PDB: 2F3Y) [16]. These structures were viewed and edited in PyMol, version 4.40 (http://www.pymol.org/) using the mutation function to alter the sequences to match the *S. mansoni* ones. The resulting SmCaM1 and SmCaM2 models were then saved as new molecules, and then computationally solvated and energy minimised using the YASARA [48]. To validate the models, Ramachandran plots were calculated using RAMPAGE (http://mordred.bioc.cam.ac.uk/~rapper/rampage.php) [53].

Expression and purification of SmCaM1 and SmCaM2

Expression vectors for *S. mansoni* calmodulins (SmCaM1 and SmCaM2) were generated by ligation independent cloning into pET-46 Ek/LIC (Merck, Nottingham, UK). This vector introduces nucleotides encoding a hexahistidine tag (amino acid sequence MAHHHHHHVDDDDK) into the coding sequence. Amplicons were generated by PCR from *S. mansoni* adult-stage cDNA (Schistosomiasis Resource Centre, distributed by BEI Resources, Manassas, VA, USA; Strain PR-1; NR-48633; Lot 62506671) using primers designed according to the manufacturer's instructions. These amplicons were purified and inserted into the vector using the manufacturer's protocol. DNA

sequences were verified (GATC Biotech, London).

Recombinant *S. mansoni* calmodulin proteins were expressed in *E. coli* Rosetta(DE3) (Merck). Competent cells were transformed according to the manufacturer's instructions, and plated overnight on LB-agar plates supplemented with 100 µg ml^{-1} ampicillin, and 34 µg ml^{-1} chloramphenicol. For the recombinant expression of both SmCaM1 and SmCaM2, single colonies were picked and cultured overnight, shaking at 30 °C, in 5 ml of LB (Miller) broth (Foremedium, UK), supplemented with 100 µg ml^{-1} ampicillin and 34 µg ml^{-1} chloramphenicol. These cultures were used to inoculate larger cultures (1 L LB broth, supplemented with 100 µg ml^{-1} ampicillin and 34 µg ml^{-1} chloramphenicol), which were grown at 22 °C for a further 10 hours before induction with 0.4 g IPTG (1.7 mM final concentration). IPTG-induced cultures were grown overnight at 16 °C, and cells harvested by centrifugation at 4200 g for 30 min. Pellets were resuspended in approximately 20 ml of buffer R (50 mM Hepes-OH, pH 7.5; 150 mM sodium chloride; 10 % (v/v) glycerol), and frozen at - 80 °C until required.

Recombinant proteins were purified by cobalt affinity chromatography, as previously described [54]. Briefly, cells were thawed, disrupted by sonication (five 30 s pulses at 100 W, separated by 30 s intervals to prevent overheating), and the suspension clarified by centrifugation (22,000 g for 20 min). The sonicate was passed through a 1 ml cobalt-agarose column under gravity (His-Select, Sigma, Poole, UK), which had been equilibrated in buffer A (50 mM Hepes-OH, pH 7.5; 500 mM sodium chloride; 10 % (v/v) glycerol). The column was washed with approximately 40 ml of buffer A, and recombinant proteins were eluted with two 2 ml aliquots of buffer C (buffer A supplemented with 250 mM imidazole). Protein fractions were dialysed overnight (on ice) in 1 L of dialysis buffer (50 mM Hepes-OH, pH 7.5; 150 mM sodium chloride; 1 mM DTT; 10 % (v/v) glycerol.). Dialysed protein samples were then aliquoted, and frozen at -80 °C until required. Once thawed, protein

stocks were either used immediately or discarded. Protein concentration was determined by the method of Bradford, using bovine serum albumin (BSA) as a standard [55].

Expression and purification of other proteins

The coding sequence for *Fasciola hepatica* calmodulin, FhCaM1 (GenBank: AM412546), was PCR-amplified from adult *F. hepatica* cDNA and inserted into pET-46 Ek/LIC. The production of plasmids for the expression of human calmodulin (HsCaM) (GenBank: AAD45181) and human galactokinase (HsGALK1) (RefSeq accession: NP_000145) has been described previously [56, 57]. These proteins were expressed and purified essentially as described for SmCaM1 and SmCaM2.

Native gel electrophoresis

In accordance with previous studies, the calcium chelator, EGTA, was routinely used to remove endogenously bound calcium ions from protein preparations: SmCaM proteins were then reconstituted with metal ions in a two-fold molar excess to ensure saturating binding conditions [54, 58-62]. For ion-binding assays, protein aliquots (10-40 µM) were incubated at 22 °C for 30 min in the presence of either EGTA, or EGTA and a two-molar excess of the appropriate ion solution, and diluted in Buffer R to a final volume of 10 µl. After this time, 10 µl of the appropriate native loading buffer was added (20 % (v/v) native running buffer pH 6.6; 20 % (v/v) glycerol; 5 % (w/v) bromophenol blue; 1 %(w/v) DTT). The protein samples were then electrophoresed at 20 mA (constant current) on 15 % continuous native-polyacrylamide gels at pH 6.6 (25 mM histidine, 30 mM MOPS) with a run-time of approximately 1 h.

For SmIQ peptide-binding assays, SmCaM1, SmCaM2, human calmodulin (HsCaM1), and *F. hepatica* calmodulin (FhCaM1) (10 µM), were incubated for 30 min at 20 °C in the presence of either EGTA (2 mM), or EGTA (2 mM)/calcium chloride (4 mM). After this time, the appropriate peptide solution (5-

160 µM) was added, and samples were incubated for a further 60 min before the addition of native loading buffer and electrophoresis on 15 % continuous native-PAGE at pH 6.6. Assays with the control protein, HsGALK1, were performed under similar conditions, except this protein was resolved under 10 % discontinuous native-PAGE at pH 8.8 (25 mM Tris-HCl, 250 mM glycine). For drug inhibition assays, SmCaM1 and SmCaM2 (10 µM), were incubated in the presence of EGTA (2 mM) and calcium chloride (4 mM) for 30 min at 20 °C, prior to the addition of SmIQ3 (20 µM), and the appropriate drug (100-600 µM in DMSO). DMSO controls (1% (v/v)) were performed under the same conditions. Samples were then incubated for a further 1 h before the addition of native loading buffer and electrophoresed under the same conditions as ion-binding assays.

Gels were stained with Coomassie blue (0.25% (w/v) Coomassie Brilliant Blue R250 dissolved in 10% (v/v) acetic acid/45% (v/v) ethanol) for at least 1 h and then destained (5% (v/v) ethanol; 7.5% (v/v) acetic acid) until the background was clear.

Analytical gel filtration

Analytical gel filtration was performed as previously described [63]. Briefly, protein samples (260-300 µl) were incubated at 20 °C for 15 min in the presence of buffer R, supplemented with either EGTA (2 mM) or calcium chloride (2 mM). Samples were then chromatographed on a Sephacryl S-300 column (Pharmacia) of total volume (V_t) 73.8 ml, which had been equilibrated with the appropriate buffer. Flow rates were fixed at approximately 0.6 – 1.0 ml min^{-1}. Fractions (0.6 – 1.0 ml) were collected, weighed and analysed for protein content using the method of Bradford [55]. These values were plotted against the running volume, and the elution volume (V_e) was determined from the absorbance maximum on the resulting chromatogram. Standard proteins, with known molecular mass (kDa) and Stoke's radii (R_s), were used to calibrate the column: serum albumin (67.0 kDa; R_s = 2.55 nm), chymotrypsinogen (25.0 kDa; R_s = 2.09 nm) and ribonuclease (13.7 kDa; R_s = 1.64

nm) (GE Healthcare). Their elution volumes (V_e) were used to calculate partition coefficients (K_{av}), according to the following equation: $K_{av} = (V_e - V_0) / (V_t - V_0)$, where V_0 is the void volume (18.5 ml, as determined using blue dextran) (GE Healthcare). These values were then plotted against R_s values, so that unknown Stoke's radii could be interpolated from the standard curve using linear regression, as implemented in GraphPad Prism, v6.0 (GraphPad Software Inc, CA, USA). To correct for the effects of hydrodynamic volume, sedimentation coefficients ($S_{20,\,w}$) were determined *in silico*, by submitting the corresponding homology model to WinHydroPRO 1.00 (http://leonardo.inf.um.es/macromol/programs/hydropro/hydropro.htm) [64]. Sub-unit stoichiometry (*n*) was then estimated using the following equation: $nM = S_{20,\,w}\, N_A\, (6\pi\eta\, R_s)/ (1 - \nu_2\rho)$, where M is the molecular mass (in Daltons), N_A is Avogadro's number (6.023×10^{23} mol^{-1}), η is the viscosity of the solvent (0.01 g cm^{-1} s^{-1}), ν_2 is the partial specific volume (0.73 g cm^3 g^{-1}), and ρ is the density of the solvent (1.0 g cm^{-3}) [65, 66].

Fluorescence spectroscopy

Intrinsic fluorescence data were collected on a Spectra Max Gemini XS fluorescence plate-reader, using SOFTmax PRO software. Excitation was set to 280 nm or 290 nm and emission spectra were collected from 330 to 400 nm. All samples were prepared in 10 mM Hepes buffer pH 7.4, supplemented with DTT (1 mM). Measurements were performed in triplicate, in 96-well black plates, and spectra were background-corrected using control samples with the appropriate buffer solution.

For peptide-binding assays, SmIQ3 peptide (14 µM) was titrated with SmCaM1 or SmCaM2 (2-28 µM) either in the presence of EGTA (0.5 mM), or in the presence of EGTA (0.5 mM)/calcium chloride (1.0 mM). Mixtures were incubated for 1.5 h at 37 °C, before analysis. Control assays with HsGALK1 (10 µM) were run alongside. Since SmCaM interactions caused a shift in peptide emission spectra,

as well as a change in fluorescence intensity, the extent of binding was not proportional to changes in the fluorescence signal at any given wavelength. Thus, spectra were integrated from 330 to 400 nm, and fluorescence data normalised by dividing the total area under the spectrum in the absence of quencher (F_0), by the total are under the spectrum at each titration point (F) [67]. Fluorescence data were analysed according to the following linear Stern-Volmer equation: $F_0/F = 1 + K_{sv}$ [Q], where [Q] is the concentration of quencher (either SmCaM1 or SmCaM2) and K_{sv} is the Stern-Volmer quenching constant [68]. Linear regressions were implemented in GraphPad Prism, v6.0.

Anilinonaphthalene-8-sulfonate (ANS; Sigma Aldrich, Poole, UK) is a fluorescent probe which binds preferentially to surface-exposed hydrophobic regions of proteins [69]. ANS fluorescence data were collected with excitation set to 350 nm, and emission spectra collected from 410 to 510 nm. Measurements were performed in triplicate, in 96-well black plates, and spectra were background-corrected using control samples with the appropriate buffer solution. Stock solutions of ANS were prepared in sterile, deionized water, and shielded from light at all times; working dilutions were prepared in 10 mM Hepes buffer pH 7.4. SmCaM1 and SmCaM2 (10 µM), were incubated for 30 min at 37 ℃ in Hepes buffer (10 mM, pH 7.4), supplemented with either EGTA (2 mM), or EGTA (2 mM) and the appropriate ion solution (4 mM). After this time ANS (36 µM) was added to each well, to a final volume of 100 µl. Samples were mixed, covered (to eliminate direct light), and incubated for a further 60 min at 37 ℃.

Statistical analysis

Datasets were analysed by one-way ANOVA with statistical significance thresholds set at $P < 0.05$ and $P \leq 0.01$. All analyses were performed in GraphPad Prism 6 using Tukey's *post hoc* test for multiple comparisons. Linear regression data were analysed by analysis of covariance (ANCOVA).

Results

Predicted structures of SmCaM1 and SmCaM2

The globular lobes of calmodulins are typically connected by a central "linker helix", of approximately eight turns in length. As this region displays considerable conformational flexibility in solution, CaM can adopt an array of conformations under different cellular conditions [70-73]. In the apo form CaM adopts a compact, "closed" conformation, whereby hydrophobic patches at the N- and C-terminal lobes are sequestered from the surrounding solvent [1, 74]. As the cellular concentration of calcium ions rises, binding at each EF-site elicits a structural rearrangement of the flanking helices; the central linker helix extends, and hydrophobic clefts are exposed at the N- and C-terminal lobes [3, 50]. Thus, calcium-saturated calmodulin (Ca^{2+}-CaM) adopts an elongated, "open" conformation. However, these conformational states are not static structures. Ca^{2+}-CaM exists in a dynamic equilibrium between the elongated conformation and a compact, or "collapsed", conformation. The latter represents a lower entropy state associated with ligand binding [51]. Transitions between these conformational states (and numerous intermediate/partially bound states) are achieved *via* structural alterations at the short connecting loop, which joins the N- and C-terminals of the linker helix [51, 75].

SmCaM homology models were constructed to mimic each of these conformational states (Fig. 1). Ca^{2+}-SmCaM proteins were modelled in the "open" conformation, as this reflects the experimentally determined structure of vertebrate CaM in the presence of excess calcium (PDB: 3CLN) [50]; and in the "collapsed" conformation, based on the bovine brain calmodulin structure (PDB: 1PRW) [51], as this is likely to represent the intermediate state of Ca^{2+}-CaM, upon interaction with binding partners and/ or antagonists. Apo-SmCaM proteins were modelled in the "closed" conformation (Fig. 1), thereby reflecting nuclear magnetic resonance (NMR) studies, which indicated that the terminal lobes of CaM adopted a globular conformation in the absence of calcium ions [6]. Furthermore, as

vertebrate CaM has been shown to form compact dimers in the absence of calcium ions (PDB: 1QX5) [52], SmCaM proteins were also modelled as homodimers. Ca^{2+}-SmCaM structures, modelled in the "open" conformation, aligned well with the template structure (with an average root mean square deviation, rmsd of 0.455 Å, over approximately 875 equivalent atoms), and with each other (with an rmsd of 0.349 Å, over 1941 equivalent atoms). The same was true of Ca^{2+}-SmCaM proteins modelled in the "collapsed" conformation, which showed high structural similarity to the template (with an average rmsd of 0.254 Å, over approximately 828 equivalent atoms), and to each other (with an rmsd of 0.264 Å, over 1050 equivalent atoms). Dimeric models also aligned well with the template structure (with an average rmsd of 0.507 Å, over approximately 1815 equivalent atoms), and with each other (with an rmsd of 0.367 Å, over 3880 equivalent atoms), as did apo-SmCaM monomers (with an rmsd of 0.551 Å, over 1840 equivalent atoms).

Examination of the Ramachandran plots for each calcium-bound structure showed that 99.3 % of residues were in "favoured" regions of the plot, whereas only 0.7 % were in "allowed" regions. Likewise, Ramachandran plots for each apo-SmCaM structure indicated that, on average, 98.5 (± 0.3) % of residues were in favoured regions of the plot, and 1.6 (± 0.3) % were in allowed regions. Although there were no "outliers" in any of the homology models analysed, it should be noted that the *X* coordinating position of the SmCaM EF-2 site was positioned within an allowed region of the plot in most structures (data not shown), thereby suggesting that the second EF-hand may be distorted from the ideal conformation around this position.

Expression and purification of SmCaM1 and SmCaM2

The two *Schistosoma mansoni* calmodulins (SmCaM1 and SmCaM2) were expressed in, and purified from, *Escherichia coli* Rosetta(DE3) cells, with protein yields of approximately 6 mg of purified protein per litre of bacterial culture (Figure 2). For comparative purposes, similar protocols were

employed successfully for the expression and purification of the *Fasciola hepatica* calmodulin, FhCaM1, and the *Homo sapiens* calmodulin, HsCaM (data not shown).

Ion binding properties of SmCaM1 and SmCaM2

Numerous studies have demonstrated that vertebrate CaM can be activated by a range of metal ions, besides calcium [76-81]. Thus, the ion binding properties of *S. mansoni* calmodulins (SmCaM1 and SmCaM2) were investigated. Native-PAGE assays revealed that the electrophoretic mobility of SmCaM1 and SmCaM2 was increased in the presence of EGTA (compared to untreated protein samples), whereas the addition of calcium ions to the EGTA treatment group reduced the electrophoretic mobility of each protein to that of the untreated sample (Fig. 3a). This suggested that both SmCaM proteins had pre-associated with calcium ions during the expression/ purification process, and that both were capable of reversibly binding this ion under the conditions of the assay. In addition to calcium ions, SmCaM1 and SmCaM2 were shown to interact with cadmium, manganese, iron and lead ions (Fig. 3a). No ion interactions could be detected in the presence of magnesium, strontium, barium, cobalt, copper, nickel, zinc or potassium under the conditions of this assay.

Previous structural studies have demonstrated that vertebrate CaM transitions from a globular "closed" conformation to an extended "open" conformation as calcium ions reach saturating levels [3, 50]. This structural transition is characterised by an increase in surface hydrophobicity at the N- and C-terminal lobes of the protein [74]. Thus, ANS fluorescence methodologies were employed to ascertain whether similar calcium-dependent conformational changes occur in *S. mansoni* calmodulins, thereby validating the choice of template structures for SmCaM homology models, and informing subsequent analytical gel filtration experiments. Since SmCaM1 and SmCaM2 were observed to bind cadmium, manganese, iron and lead ions in native-PAGE assays (Fig. 3a), these

ions were included in ANS fluorescence experiments; whereas magnesium (which had no observable effect on the electrophoretic mobility of either protein) (Fig. 3a), was included as a negative control.

ANS displayed the expected fluorescence emission spectrum when incubated in the presence of SmCaM1 or SmCaM2, and excited at 350 nm: a broad peak was observed, with a fluorescence intensity maximum (λ_{max}) at approximately 460 nm (Fig. 3b). When SmCaM proteins were incubated with ANS in the presence of EGTA, the fluorescence intensity at λ_{max} was lower than that of the calcium treatment group, thereby suggesting that calcium chelation caused structural rearrangement in each protein, characterised by a net gain in surface hydrophobicity. This observation is consistent with a structural transition from the "closed" to the "open" conformation. A similar effect was observed with cadmium, manganese, iron and lead ions, but not with magnesium ions (Fig. 3b), reflecting the ion binding patterns of SmCaM1 and SmCaM2 under non-denaturing native-PAGE (Fig. 3a). Interestingly, these results showed a difference from those obtained by native gel electrophoresis. While the untreated and EGTA-treated proteins had different mobilities on native gels, they had quite similar ANS fluorescence spectra (with the EGTA-treated proteins having only marginally lower fluorescence intensity). The explanation for this is not completely clear. It may reflect the nature of the purified, recombinant proteins. It is possible that the recombinant proteins bind calcium resulting in an overall change in shape and charge (reported in the native gel assay), and the exposed hydrophobic patches associate with non-polar bacterial molecules (e.g. membrane lipids which will be released when the cells are disrupted during purification) which block the association of ANS. EGTA treatment would remove the calcium ions, reverse the exposure of the hydrophobic regions and release any bound hydrophobic molecules (which would be diluted to be much lower concentration in the assays than during purification).

Dimerisation of SmCaM proteins

Previous studies have demonstrated that vertebrate CaM forms non-covalently linked homodimers in the apo-state [52, 82]. Analytical gel filtration methodologies were employed to estimate the oligomeric state of *S. mansoni* calmodulins in the presence and absence of calcium ions. Since human galactokinase (HsGALK1), exists predominantly as a monomer *in vitro* [57], this protein was used as an internal control. Examination of the elution profiles, revealed that SmCaM1 and SmCaM2 eluted at a lower volume in the presence of 2 mM EGTA, than in the presence of 2 mM calcium chloride, implying that oligomerisation was promoted in the absence of calcium ions. Indeed, apo-SmCaM proteins eluted at approximately twice the molecular mass of their calcium-bound counterparts, yielding taller and sharper elution peaks than those observed in the presence of calcium ions (Fig. 4). This indicated a shift from the dimeric to the monomeric state upon calcium chelation, accompanied by an increase in conformational heterogeneity. The molecular mass of the control protein (HsGALK1) was estimated at approximately 42 kDa using this method; this is consistent with the molecular mass of the HsGALK1 monomer (43 kDa as estimated from the primary sequence of the hexahistidine-tagged recombinant form).

However, the results from ANS fluorescence assays suggest substantial conformational changes on ion binding and unbinding. To correct for any possible effects of these changes on the elution profiles, sedimentation coefficients were computationally estimated from SmCaM homology models using WinHydroPRO v1.00 [64]. Ca^{2+}-SmCaM structures (modelled in the "open" conformation), generated computationally estimated sedimentation coefficients of 1.69 S for Ca^{2+}-SmCaM1, and 1.67 S for Ca^{2+}-SmCaM2; whereas dimeric models generated sedimentation coefficients of 2.87 – 2.89 S (Table 1). Stoke's radii (R_s) were estimated from the gel filtration data as 2.47 nm for Ca^{2+}-SmCaM1, and 2.61 nm Ca^{2+}-SmCaM2. These values yielded an estimated subunit stoichiometry of 0.95 – 0.99 for the SmCaM monomers, and 1.61 – 1.71 for the SmCaM dimers

(Table 1). Given that monomeric models represented a better fit to the experimental data than dimeric models, this provided further evidence that both SmCaM proteins eluted as monomers in the presence of calcium ions. Conversely, apo-SmCaM structures (modelled in the "closed" conformation), generated computationally estimated sedimentation coefficients of 1.82 S for apo-SmCaM1, and 1.83 S for apo-SmCaM2 (Table 1). Both proteins had an R_s value of 3.29 nm and this yielded a subunit composition of approximately 1.4 for the SmCaM monomer, and 2.15 - 2.16 for the SmCaM dimer (Table 1). As dimeric models represented a better fit to the experimental data than monomeric models, this provided further evidence that SmCaM proteins eluted as homodimers in the absence of calcium ions. The same methodologies were applied to the control protein, HsGALK1, which was modelled as a monomer and as a dimer, using the experimentally determined structure (PDB: 1WUU) [83]. Monomeric HsGALK1 yielded an estimated subunit stoichiometry of approximately 0.98, whereas the HsGALK1 dimer yielded a subunit composition of approximately 1.5 (Table 1). As expected, the monomeric model represented a better fit to the experimental data, thereby validating the analytical methods employed in this study.

Identification of IQ-motifs in S. mansoni voltage-gated calcium channels

Ca_v α_1 subunits contain a conserved, α-helical motif directly termed the isoleucine-glutamine (IQ) motif. The IQ motif spans a region of approximately 20 amino acids, but the core of the motif is defined by an 11-residue consensus sequence, IQxxxBxxxxB, where B signifies a positively charged amino acid residue (arginine or lysine), and x signifies a variable amino acid [11]. The IQ motif is a known binding site for CaM. Indeed, the $Ca_v1.2$ channel IQ domain been implicated as a possible tethering site for apo-CaM [84], whereas numerous studies have shown that Ca^{2+}-CaM interactions with the IQ domain are essential for the CDI and CDF of both Ca_v1-type and Ca_v2-type channels [85, 86]. Moreover, crystallographic studies have demonstrated that the affinity and orientation of the Ca^{2+}-CaM-Ca_v IQ domain interaction is dictated by the overall charge distribution of the IQ motif, as

well as the spacing and positioning of key hydrophobic/aromatic "anchor" residues [16, 17, 87, 88].

We identified four IQ-motifs in *S. mansoni* Ca_v α_1 subunits and designated SmIQ1 - SmIQ4 (Fig. 5), which display an unusual pattern of distribution. For instance, whereas SmIQ1, SmIQ3 and SmIQ4 are each "conventionally" positioned within the C-terminal regions of $SmCa_v1A$, $SmCa_v1B$ and $SmCa_v2A$, respectively (Fig. 5), $SmCa_v2B$ seemingly lacks an IQ motif, containing a stop codon directly upstream from the expected position of the IQ consensus sequence [26]. Furthermore, the $SmCa_v1A$ α_1 subunit contains a second IQ motif (SmIQ2) directly following the first [26], resulting in an unusually extended IQ domain. Although IQ motifs often occur as tandem repeats in the muscle protein myosin [11], this phenomenon is not commonly observed in Ca_v channels, and appears to be unique to parasitic flatworms. Based on these sequence analyses, synthetic peptides (23-mers) were designed to incorporate the four IQ-motifs (bold sequences in Fig. 5).

Interaction of SmCaM1 and SmCaM2 with IQ-motifs from voltage-gated calcium channels

Native-PAGE assays revealed that the electrophoretic mobility of SmCaM1 and SmCaM2 was decreased in the presence of SmIQ3 (compared to the untreated protein sample) (Fig. 6a). These effects occurred both in the presence and absence of calcium ions, but could not be detected in the presence of SmIQ1, SmIQ2 or SmIQ4, nor in the presence of the control protein, HsGALK1 (Fig. 6a), thereby implying a specific, calcium-independent interaction between both *S. mansoni* calmodulins and SmIQ3. Moreover, as interactions were resolved as discrete shifts on native gels, this indicated the formation of a stable, long-lived binding complex with the SmIQ3 peptide. A similar outcome was observed in native-PAGE assays with the *F. hepatica* calmodulin, FhCaM1, and vertebrate CaM (as exemplified by the human isotype, HsCaM) (Fig. 6a), indicating that the SmIQ3 peptide forms a stable binding complex with generic, 148-amino acid calmodulins from distant phyla.

Semi-quantitative native-PAGE confirmed the occurrence of a dose-dependent interaction between SmCaM1 or SmCaM2 and the SmIQ3 peptide (Fig. 6b). As expected, both calmodulin isotypes underwent a similar reciprocal exchange from the higher- to the lower-mobility species, with increasing concentrations of SmIQ3 (Fig. 6b), indicating a comparable affinity for the peptide. These effects were absent in assays with SmIQ1, SmIQ2 or SmIQ4 (data not shown). However, whereas the graded transition from the higher- to the lower-mobility state resulted in the disappearance of the unbound protein band at a 1:4 (protein:peptide) molar ratio in the presence of EGTA (2 mM), this interchange occurred at a 1:2 (protein:peptide) molar ratio in the presence of a 2-fold molar excess of calcium chloride (Fig. 6b). This suggests that both SmCaM proteins may have a marginally lower affinity for SmIQ3 in the apo-state, than they do in the calcium-bound state.

As the two SmCaM proteins do not contain tryptophan residues, they emit negligible fluorescence when excited at wavelengths within the 280 to 295 nm range. Therefore, in intrinsic binding assays with SmIQ3, the bulk of the fluorescence signal can be attributed to two tryptophan residues, located at positions 3 and 7 of the SmIQ3 peptide. Initial tryptophan fluorescence assays utilised an excitation wavelength of 295 nm, to limit interference from SmCaM tyrosine residues [68]. However, these preliminary experiments resulted in complete quenching of the SmIQ3 fluorescence signal upon addition of SmCaM1/ SmCaM2, which could not be accurately quantified (data not shown). Thus, excitation was set to 280 nm, and emission measured from 330 to 400 nm. The SmIQ3 peptide yielded a characteristic fluorescence emission spectrum, when excited at 280 nm. A broad peak was observed, with a fluorescence emission intensity maximum (λ_{max}) at approximately 355 nm (Fig. 7). When SmIQ3 was titrated with increasing concentrations of SmCaM1 or SmCaM2, the fluorescence intensity at λ_{max} was substantially lower than that of the untreated peptide (Fig. 7). These effects were dose-dependent, and occurred both in the presence and absence of calcium ions, implying that the two tryptophan residues of the peptide had come into close contact with

quenching groups, located within the protein. This, in turn, was consistent with a net reduction in solvent-exposed (free) peptide. Fluorescence quenching also caused a blue-shift in emission spectra, yielding broader, flatter peaks than those observed in the presence of free peptide (Fig. 7), thereby implying that SmIQ3 was positioned in a more hydrophobic environment upon binding SmCaM1 or SmCaM2 [68]. These data are consistent with assimilation of the peptide within the CaM hydrophobic pocket, leading to the formation of a compact binding complex.

Since native-PAGE assays had suggested that *S. mansoni* calmodulins had a higher affinity for SmIQ3 in the presence of calcium ions, than they did in the apo-state (Fig. 6b), intrinsic fluorescence data were quantified according to the Stern-Volmer (SV) relationship (Fig. 7). Briefly, fractional fluorescence was plotted as a function of SmCaM concentration, to quantify the change in SmIQ3 fluorescence resulting from complex formation [68], and the strength of the interaction between the quencher (SmCaM1 or SmCaM2) and fluorophore (SmIQ3) was reported as the SV quenching constant (K_{sv}), which was determined from the slope of the resulting linear plot (Table 2). It should be noted that K_{sv} contains both static (complex-forming) and dynamic (collisional) components [68]. However, since native-PAGE experiments had indicated that SmCaM proteins formed a stable binding complex with the SmIQ3 peptide (Fig. 6), fluorescence datasets were considered to represent primarily static quenching. Indeed, the linear nature of each SV plot suggested that static quenching was dominant in the system (Fig. 7), with negligible contributions from dynamic/ collisional quenching. In this scenario, K_{sv} can be assumed to be equal to the association constant (K_a) between the fluorophore and quencher [68]. Statistical analysis of the linear regression of the SV data, demonstrated a significant difference between treatment groups ($p < 0.001$; ANCOVA; $n = 3$), which, upon analysis of the K_{sv} association constant for each treatment group, represented a small, but significant increase in SmCaM-SmIQ3 affinity in the presence of calcium ions, compared to the EGTA treatment group ($p < 0.05$; ANOVA; $n = 3$) (Table 2). This provided further indication

that SmIQ3 binding was promoted in the presence of calcium ions. Furthermore, as K_{sv} association constants for complex formation were not significantly different between SmCaM1 and SmCaM2 datasets (Table 2), suggesting that both calmodulins had a comparable affinity for the SmIQ3 peptide.

Non-denaturing native-PAGE was used to screen for interactions between SmCaM proteins and the calmodulin antagonists, CPZ, W7, TFP and ThA (Fig. 8a). As the actions of these calmodulin antagonists have been shown to be calcium-dependent [89, 90], binding assays were performed under calcium-saturating conditions. Thus, in each gel image, higher-mobility bands correspond to Ca^{2+}-SmCaM, whereas lower-mobility bands represent the Ca^{2+}-SmCaM-SmIQ3 complex (Fig. 8a). Given that previous studies have indicated that the antischistosomal drug, PZQ, interacts with a myosin regulatory light chain (MLC), which bears certain structural similarity to calmodulin [91], this drug was tested alongside the others (Fig. 8a). Both calmodulins underwent a partial exchange from the lower- to the higher-mobility species, in the presence of CPZ and TFP (Fig. 8a), implying an inhibitory effect on protein-peptide interactions. These inhibitory effects could not be detected in the presence of PZQ, W7 or ThA, nor in the presence of the delivery vehicle, DMSO (Fig. 8a), indicating a specific interaction with the phenothiazine drugs, CPZ and TFP. Moreover, semi-quantitative native-PAGE assays demonstrated that both SmCaM proteins underwent a graded exchange from the lower- to the higher-mobility species with increasing concentrations of CPZ or TFP, consistent with a dose-dependent antagonism of the SmCaM-SmIQ3 binding complex (Fig. 8b).

Discussion

The two calmodulins of *S. mansoni* have very similar biochemical properties. In the experiments described here no differences in ion binding, conformational change in response to ions, dimerization, IQ-motif binding or antagonism of this binding was detected. Given the highly similar

sequences, this might be expected. Nevertheless, it raises the question as to why the organism expresses two highly similar isotypes of the same protein from two separate genes. Previous work has demonstrated that both isotypes are expressed in the same life cycle stages [43]. This suggests that the two isotypes do not have stage-specific roles as has been suggested for the tegumental allergen-like proteins from this species or the β-tubulin isotypes in *F. hepatica* [92-94]. The *S. mansoni* calmodulins also show some differences in properties to the proteins from other trematodes. *F. hepatica* expresses at least three calmodulin isotypes [95, 96]. Of these, FhCaM1 is the most similar to SmCaM1 and SmCaM2 in sequence and predicted structure. However, this protein (and FhCaM2) interacts with magnesium ions in native gel electrophoresis, unlike SmCaM1 and SmCaM2 [95]. *Clonorchis sinensis* calmodulin also interacts with both calcium and magnesium ions [97]. There is also no evidence for dimerization of FhCaM1, although there is some evidence from gel electrophoresis for dimerization of FhCaM3 [96]. TFP and W7 both interact with FhCaM1 and FhCaM3, but not FhCaM2 [96]. In this work, we demonstrated that FhCaM1 (and HsCaM) also bound to the SmIQ3 peptide. Identical sequences occur in voltage-gated calcium channels in *Opisthorchis viverrini*, *Clonorchis sinensis* and *Echinococcus granulosus* suggesting that these also represent sites for calmodulin binding in these parasites. FhCaM1 also interacts with a sequence from a plasma membrane calcium ATPase (PMCA). This sequence is predicted to adopt an α-helical conformation, but it is not an IQ-motif [98]. Therefore, it seems likely that SmCaM1 and SmCaM2 also bind to (and, most likely, regulate) PMCA in addition to voltage-gated calcium channels.

Despite containing three L-type Ca_v channel IQ motifs (SmIQ1, SmIQ2 and SmIQ3) (Fig. 5), bioinformatics data suggest that only two of these sequences represent functional binding sites for CaM. SmIQ1 and SmIQ3 are 100% conserved in trematodes, and share considerable (75 %) sequence identity with the IQ motifs of mammalian L-type, $Ca_v1.2$ channels. Both motifs adhere to the IQ consensus sequence, and both contain a full complement of six aromatic anchors. Moreover,

structure prediction using Phyre2 predicted a high α-helical propensity for both IQ sequences, a structural characteristic common to many CaM target sites [99]. Conversely, SmIQ2 is not well conserved in platyhelminths, and bears little resemblance to the IQ motifs of mammalian Ca_v1-type channels. Indeed, this vestigial sequence contains a one residue deletion at position four, a conspicuous paucity of aromatic anchors, and (according to structure prediction by Phyre2) a largely disordered secondary structure (data not shown). Thus, whereas SmIQ1 and SmIQ3 seemingly fit the criteria for a canonical CaM binding site, it may be hypothesised that SmIQ2 has either lost the ability to bind calmodulin, or does so *via* a novel, non-canonical anchoring scheme. Interestingly, the sole non-L-type Ca_v channel IQ motif in *S. mansoni* (SmIQ4) also deviates considerably from the IQ consensus sequence (Fig. 5). Indeed, this unusual motif may span either one of two overlapping positions. For example, multiple sequence alignments indicate that the core of the SmIQ4 consensus sequence begins with the isoleucine residue at position 0 (i.e ^{1581}IYENWQMNKST^{1591}). In this scenario, a lack of positively charged amino acids means that SmIQ4 has a net charge of zero (whereas mammalian Ca_v2 channel IQ motifs typically have a net charge of +1 or +2). Moreover, four (out of five) critical residues of the IQ consensus sequence are lost, including the central and terminal basic residues of the motif, and a conserved aromatic anchor at position three which has been shown to be energetically important for Ca^{2+}-CaM binding in mammalian Ca_v2-type channels [87]. Alternatively, given that the first position of the IQ motif is ambiguous for a hydrophobic or aromatic residue in myosin proteins [11], the core of the SmIQ4 consensus sequence could begin with the tryptophan residue at position four (i.e. ^{1585}WQMNKSTGNKK^{1595}). In this scenario, the distribution of anchoring positions is disrupted, but the motif has a more conventional charge distribution (with a net charge of +3), and two (out of five) positions of the IQ consensus sequence are maintained.

The lack of binding between SmCaM and IQ1 was, therefore, unexpected. Native-PAGE assays tend

to detect binding events which are stably maintained throughout the duration of the experiment, and fluorescence quenching relies on changes to the environment of fluorescent amino acid residues to infer binding. Therefore it is possible that some SmIQ peptides interact with calmodulin in a way which involves rapid association and dissociation combined with binding in a way which does not affect the environment of a fluorophore. It is also possible that high affinity binding with calmodulin to some of the IQ-motifs requires additional sequences from the protein, which are not present in the relatively short peptides used here. Nevertheless, given that SmIQ1 and SmIQ3 differ from each other by four "variable" positions of the consensus sequence (at positions 2, 6, 8 and 9), and that three of these positions distinguish the SmIQ1 sequence from higher-affinity sites, such as the $Ca_v1.2$ IQ motif (or SmIQ3) (Fig. 5), it is possible to speculate that these substitutions endow the SmIQ1 peptide with an inherently lower affinity for CaM.

Vertebrate CaM can be antagonised by a range of drugs, some of which are used in a clinical setting for the treatment of psychiatric disorders [100]. For example, the antipsychotic drug chlorpromazine (CPZ), has been shown to bind to multiple sites on the CaM structure [89], antagonising the protein's function in a dose-dependent manner [101, 102]. Similar effects were observed with the phenothiazine derivative, trifluoperazine (TFP) [90, 103]. Indeed, structural studies of the TFP-CaM binding complex have demonstrated that at least one drug molecule binds within a large "V-shaped" hydrophobic binding pocket, formed by the collapse of the N-and C-terminal lobes of the protein [103, 104]; stabilising a compact conformation that occludes interactions with peptide ligands [103, 105]. Furthermore, *in vitro* bioassays have demonstrated an enhanced motility/ stunted growth phenotype in *F. hepatica* juveniles treated with TFP. These effects are consistent with those observed upon silencing of calmodulin *via* RNA inactivation (RNAi) [106]. Since both CPZ and TFP were observed to antagonise SmCaM-SmIQ3 complex formation in a concentration-dependent manner (Fig. 8), this implies a druggable interaction between SmCaM and the $SmCa_v1B$ calcium

channel. Indeed, as previous studies have demonstrated that *S. mansoni* larvae react to TFP treatment *via* a dose-dependent reduction in miracidial transformations [43], it is tempting to speculate that these phenotypic effects stem, at least in part, from the inhibition of interactions between calmodulin and the IQ domain of the $SmCa_v1B$ α_1 subunit.

Given that exposure of adult *S. mansoni* worms to the antischistosomal drug, PZQ, results in disruption of calcium homeostasis [107], components of parasite calcium signalling pathways (including binding partners of CaM), have attracted considerable attention as the possible molecular targets of PZQ [39], and as putative candidates for novel treatment strategies against schistosomiasis. The biochemical analyses presented here provide no indication of an interaction between *S. mansoni* calmodulin and praziquantel. Thus, the interaction between calmodulin and the $SmCa_v1B$ calcium channel is unlikely to represent a molecular target for this drug. Moreover, the calmodulin is highly conserved through different animal phyla and there is high sequence identity between SmIQ3 and the IQ motifs of mammalian Ca_v channels. This means that the antagonism of the SmCaM-$SmCa_v1B$ complex, while possible, is unlikely to be sufficiently selective for the parasite over the host. Thus, this interaction may not represent a viable target for anthelmintic development. Nevertheless, there are important functional roles for $SmCa_v1B$ in parasite calcium signalling processes. Therefore, these observations do not eliminate the possibility that schistosome Ca_v channels represent viable candidates for the design of novel anthelmintics. Thus, proteins unique to trematodes which are involved in the functioning or regulation of these channels may represent intriguing candidates for future drug development.

Acknowledgements

CMT was in receipt of a PhD studentship from the Department of Employment and Learning, Northern Ireland (DELNI, UK).

Figure legends

Figure 1: **The predicted structures of SmCaM1 and SmCaM2.** Top: a schematic representation of the domain organisation of SmCaM proteins; N, denotes the N-terminal domain; C, denotes the C-terminal domain. Red represents the SmCaM N-lobe (residues 1-64); green represents the central helix region (residues 65-92); blue represents the SmCaM C-lobe (residues 93-148); pink represents the flexible connecting loop (residues 77-81). Protein structures are displayed in cartoon format, and calcium ions are depicted as yellow spheres. Images were constructed in PyMol, version 4.40. Apo-SmCaM1 was modelled in the "closed" state, using Phyre2 in the intensive mode [47]. Calcium-bound SmCaM1 was modelled in the "collapsed" state, using bovine CaM as a template (PDB: 1PRW) [51]. Calcium-bound SmCaM1 was also modelled in the "open" state, using *R. rattus* calmodulin as a template (PDB: 3CLN) [50]. All models were energy minimised in YASARA [48].

Figure 2: **Expression and purification of SmCaM1 and SmCaM2**. Recombinant SmCaM1 and SmCaM2 were purified from *E. coli* Rosetta(DE3) competent cells and this process was monitored by 15 % SDS-PAGE: M, molecular mass ladder (sizes in kDa to the left of the gels); U, sample from uninduced cells, prior to IPTG induction; I, sample from induced cells prior to harvesting; S, sample from soluble sonicate after clarification by centrifugation; W, samples from two washes with buffer A; E, samples from two elutions with buffer C.

Figure 3: **Ion binding by SmCaM1 and SmCaM2**. (a) SmCaM1 and SmCaM2 (10 µM) were resolved on 15 % continuous native-PAGE at pH 6.6 [108]. U, Untreated proteins (U), E, proteins treated with EGTA (2 mM). Ion-treated proteins (as indicated on the panels at the top of this figure), were incubated in the presence of 2 mM EGTA and 4 mM of the appropriate ion solution. Reduced mobility, compared to the EGTA-treated protein, is evidence of ion binding. (b) SmCaM1 and SmCaM2 (10 µM) were incubated either in the presence of EGTA (2 mM), or in the presence of EGTA

(2 mM), and the appropriate ion solution (4 mM) together with ANS (36 µM). U, untreated protein samples are shown in light blue; E, EGTA treatment group is shown in red; ion treatment groups are shown as follows: calcium (green), cadmium (purple), manganese (orange), magnesium (black), iron (brown), and lead (pink). The fluorescence spectra shown are plots the mean fluorescence intensity, measured in arbitrary units (AU), over a range of emission wavelengths. Assays were baseline corrected using an equal volume of buffer, containing the appropriate concentration of EGTA/ion solution. An increase in fluorescence intensity is associated with the exposure of hydrophobic regions on the surface of the protein, resulting from interaction with the ion and subsequent conformational change. This was seen with calcium, lead, cadmium and, to a lesser extent, iron (II) and manganese (II) ions. Magnesium ions cause almost no change in the ANS fluorescence spectra (and the line is partly obscured by that for the untreated protein) and EGTA treatment causes a modest decrease.

Figure 4: **The oligomeric state of SmCaM1 and SmCaM2 is dependent on calcium ions** The top graph shows the elution of SmCaM proteins in the presence of either EGTA (2 mM), or calcium chloride (2 mM) along with the control protein, human galactokinase (HsGALK1). Samples from each fraction were treated with Bradford's reagent, and absorbance was measured at 595 nm in order to estimate protein content. Elution volumes (V_e) were determined from absorbance maxima. Apo-SmCaM1 is shown in blue, apo-SmCaM2 in red, Ca^{2+}-SmCaM1 in green; Ca^{2+}-SmCaM2 in purple and the control protein, HsGALK1, in orange. The calibration graphs derived from data obtained using proteins of known molecular mass (M) and Stoke's radius (R_S) are shown below. R, Ribonuclease; C, Chymotrypsinogen; A, serum albumin. All calculations and analyses were performed in GraphPad Prism, version 6.0.

Figure 5: **IQ-motifs from the voltage-gated calcium channels of *Schistosoma mansoni*** Multiple

sequence alignments were generated in Mega 6.06, using MUSCLE [109]. The IQ-motifs SmIQ1 and SmIQ2 are located in the $SmCa_v1A$ α_1 subunit, SmIQ3 is located in $SmCa_v1B$, and SmIQ4 is located in $SmCa_v2A$. The numbers in parentheses denote the position of the first amino acid in each aligned sequence. The "IQ consensus" sequence (top), was derived from [110], where "x" represents any amino acid. To facilitate comparisons between different sequences, the first isoleucine residue of the IQ motif is referred to as "position 0" and other residues are numbered according to their N-terminal (-), or C-terminal (+) location, relative to position 0. Stars represent conserved "anchor" positions [17, 87]. Bold residues represent 23-mer, synthetic SmIQ peptide sequences. Accession numbers: Human $Ca_v1.1$ (AAI33672); Human $Ca_v1.2$ (AAI46847); Human $Ca_v1.3$ (AAA58402); Human $Ca_v1.4$ (NP_005174); Human $Ca_v2.1$ (O00555); Human $Ca_v2.2$ (AAA51898); Human $Ca_v2.3$ (NP_001192222); *S. mansoni* $SmCa_v1A$ (AAK84312); *S. mansoni* $SmCa_v1B$ (CCD59069); *S. mansoni* $SmCa_v2A$ (AAK84311); *S. mansoni* $SmCa_v2B$ (AAK84313).

Figure 6: **Interaction of SmCaM1 and SmCaM2 with IQ-motifs from voltage-gated calcium channels** (a) Gel images showing the migration patterns of SmCaM1 and SmCaM2 (10 µM) on 15 % continuous native-PAGE at pH 6.6 [108]. Untreated (U) SmCaM proteins, were treated with either EGTA (2 mM) (left-hand gels), or EGTA (2 mM) and calcium chloride (4 mM) (right-hand gels), in the presence of SmIQ peptides, SmIQ1, SmIQ2, SmIQ3 and SmIQ4 (labelled 1-4), at a final concentration of 160 µM. Similar protocols were applied to the *F. hepatica* calmodulin, FhCaM1 (GenBank: AM412546), and vertebrate CaM, as exemplified by the *H. sapiens* calmodulin, HsCaM (GenBank: AAD45181). *H. sapiens* galactokinase, HsGALK1 (RefSeq: NP_000145) was used as a negative control. (b) Gel images showing the migration patterns of tSmCaM1 and SmCaM2 (10 µM) on 15 % continuous native-PAGE at pH 6.6. Untreated (U) SmCaM proteins, were treated with either EGTA (2 mM), or EGTA (2 mM) and calcium chloride (4 mM) (as labelled), in the presence of rising concentrations of the SmIQ3 peptide (final concentrations 5, 10, 20, 40, 80 and 160 µM). Higher-

mobility (bottom) bands represent unbound SmCaM1 or SmCaM2; lower-mobility (top) bands represent the SmCaM-SmIQ3 peptide complex. The second lane (labelled "IQ3"), represents the peptide-only (160 µM) control. Assays with SmIQ1, SmIQ2 and SmIQ4 did not display a mobility shift under the same conditions (data not shown).

Figure 7: **Affinity of SmCaM1 and SmCaM2 with IQ-motifs from voltage-gated calcium channels** SmIQ3 peptide (14 µM) was incubated either in the presence of EGTA (0.5 mM), or in the presence of EGTA (0.5 mM)/calcium chloride (1 mM), and treated with rising concentrations of SmCaM1 or SmCaM2 (2-28 µM). U, untreated protein samples are depicted in blue. Assays were excited at 280 nm, and emission recorded from 330 to 400 nm. Intrinsic fluorescence spectra (left column) were recorded for each assay, and were baseline corrected using the appropriate buffer and concentration of SmCaM1 or SmCaM2. Since SmCaM1 and SmCaM2 both lack tryptophan residues, these spectra largely report on the environment of tryptophans in the peptides. Quenching of the fluorescence is evidence for peptide-CaM interaction. Stern-Volmer plots (right column) were used to determine fluorescence quenching constants and, subsequently, to compare the affinities of the peptides and proteins (see Results). Fractional fluorescence (F_o/F) was determined by dividing the area under the untreated (U) spectrum by the respective quenched spectrum. Linear regressions were performed in GraphPad Prism, version 6.0 (GraphPad Software Inc, CA, USA).

Figure 8: **Antagonism of the interaction of SmCaM1 and SmCaM2 with IQ-motifs by calmodulin antagonists** (a) Gel images showing the migration of SmCaM1 (top) and SmCaM2 (bottom) on 15 % continuous native-PAGE at pH 6.6 [108]. SmCaM proteins (10 µM), were treated with EGTA (2 mM) and calcium chloride (4 mM), in the presence of the SmIQ3 peptide (20 µM). The first lane represents untreated (U) SmCaM1 or SmCaM2, the second lane (IQ3), represents the untreated Ca^{2+}-SmCaM-SmIQ3 binding complex. SmCaM-SmIQ3 binding complexes were treated with DMSO

(D), at a final concentration of 1 % (v/v), or the following drugs: praziquantel (PZQ), chlorpromazine (CPZ), N-(6-Aminohexyl)-5-chloro-1-naphthalenesulfonamide hydrochloride (W7), trifluoperazine (TFP), or thiamylal (ThA), each at a final concentration of 500 µM. (b) Gel images showing the migration patterns of SmCaM1 and SmCaM2 under 15 % continuous native-PAGE at pH 6.6. SmCaM proteins (10 µM), were treated with EGTA (2 mM) and calcium chloride (4 mM), in the presence of the SmIQ3 peptide (20 µM). The first lane represents untreated (U) SmCaM1 or SmCaM2, the second lane (IQ3), represents the untreated Ca^{2+}-SmCaM-SmIQ3 binding complex. SmCaM-SmIQ3 complexes were treated with rising concentrations of either CPZ or TFP (as labelled; 0.1 to 0.6 mM, rising in increments of 0.1 mM).

Tables

Table 1: Dimerisation of SmCaM1 and SmCaM2 as determined by analytical gel filtration

	Apo-SmCaM1	Apo-SmCaM2	Ca^{2+}-SmCaM1	Ca^{2+}-SmCaM2	HsGALK1
Molecular mass determined from primary sequence, M_{seq} (kDa)					
Monomer	18.5	18.5	18.5	18.5	43.3
Dimer	37.0	37.0	37.0	37.0	86.6
Eluction volume, V_e (ml)	25.6	25.6	28.8	28.2	27.3
Stoke's radius, R_s (nm)	3.3	3.3	2.5	2.6	2.9
Sedimentation coefficient, $S_{20,w}$ (S)					
Monomer	1.8	1.8	1.7	1.7	3.5
Dimer	2.9	2.9	2.9	2.9	5.4
Estimated molecular mass, M_{est} (kDa)					
Monomer	25.2	25.3	17.6	18.3	42.3
Dimer	39.7	40.0	29.8	31.7	65.8
Stoichiometry					
Monomer	1.36	1.37	0.95	0.99	0.98

Dimer	2.15	2.16	1.61	1.71	1.52
Best fit	Dimer	Dimer	Monomer	Monomer	Monomer

Apo-SmCaM proteins were treated with EGTA (2 mM), Ca^{2+}-SmCaM proteins were treated with calcium chloride (2 mM). M_{seq} represents the molecular mass of each protein, as determined from the primary sequence, plus the N-terminal His6-tag (see Experimental section). Elution volumes (V_e) were used to determine partition coefficients (K_{av}). Stokes radii (R_s) were interpolated from the standard curve by comparison with standard proteins using linear regression. M_{est} represents the estimated molecular mass of each protein species. Sedimentation coefficients ($S_{20,\,w}$) were estimated *in silico* using WinHydroPRO v1.00 and the most relevant molecular model.

Table 2: Stern-Volmer constants for the interaction between *S. mansoni* calmodulins and SmIQ3

	Stern-Volmer constant, K_{sv} ($\times 10^4\ M^{-1}$) ± SEM	
	EGTA	**EGTA/$CaCl_2$**
SmCaM1	7.84 ± 0.49 *	11.06 ± 0.65
SmCaM2	7.51 ± 0.61 *	10.6 ± 0.34

Stern-Volmer quenching constants (K_{sv}) were determined as described in the Experimental section. K_{sv} values for SmCaM-SmIQ3 complexes in the presence of EGTA (0.5 mM) were significantly lower than those treated with EGTA (0.5 mM) and $CaCl_2$ (1.0 mM); * $p \leq 0.05$; ANOVA; n = 3.

REFERENCES

[1] D. Chin, A.R. Means, Calmodulin: a prototypical calcium sensor, Trends in cell biology, 10 (2000) 322-328.
[2] Y.S. Babu, J.S. Sack, T.J. Greenhough, C.E. Bugg, A.R. Means, W.J. Cook, Three-dimensional structure of calmodulin, Nature, 315 (1985) 37-40.
[3] R. Chattopadhyaya, W.E. Meador, A.R. Means, F.A. Quiocho, Calmodulin structure refined at 1.7 Å resolution, Journal of Molecular Biology, 228 (1992) 1177-1192.
[4] J.L. Gifford, M.P. Walsh, H.J. Vogel, Structures and metal-ion-binding properties of the Ca^{2+}-binding helix-loop-helix EF-hand motifs, The Biochemical journal, 405 (2007) 199-221.
[5] A. Lewit-Bentley, S. Rety, EF-hand calcium-binding proteins, Curr Opin Struct Biol, 10 (2000) 637-643.
[6] M. Zhang, T. Tanaka, M. Ikura, Calcium-induced conformational transition revealed by the solution structure of apo calmodulin, Nature structural biology, 2 (1995) 758-767.
[7] D.C. LaPorte, B.M. Wierman, D.R. Storm, Calcium-induced exposure of a hydrophobic surface on calmodulin, Biochemistry, 19 (1980) 3814-3819.
[8] R. Gopalakrishna, W.B. Anderson, Ca^{2+}-induced hydrophobic site on calmodulin: application for purification of calmodulin by phenyl-Sepharose affinity chromatography, Biochemical and biophysical research communications, 104 (1982) 830-836.
[9] S.W. Vetter, E. Leclerc, Novel aspects of calmodulin target recognition and activation, European journal of biochemistry / FEBS, 270 (2003) 404-414.
[10] K.L. Yap, J. Kim, K. Truong, M. Sherman, T. Yuan, M. Ikura, Calmodulin target database, Journal of structural and functional genomics, 1 (2000) 8-14.
[11] M. Bahler, A. Rhoads, Calmodulin signaling via the IQ motif, FEBS letters, 513 (2002) 107-113.
[12] H. Koide, T. Kinoshita, Y. Tanaka, S. Tanaka, N. Nagura, G. Meyer zu Horste, A. Miyagi, T. Ando, Identification of the single specific IQ motif of myosin V from which calmodulin dissociates in the presence of Ca^{2+}, Biochemistry, 45 (2006) 11598-11604.
[13] Z. Li, D.B. Sacks, Elucidation of the interaction of calmodulin with the IQ motifs of IQGAP1, Journal of Biological Chemistry, 278 (2003) 4347-4352.
[14] S.R. Martin, P.M. Bayley, Calmodulin bridging of IQ motifs in myosin-V, FEBS letters, 567 (2004) 166-170.
[15] I. Rayment, W.R. Rypniewski, K. Schmidt-Base, R. Smith, D.R. Tomchick, M.M. Benning, D.A. Winkelmann, G. Wesenberg, H.M. Holden, Three-dimensional structure of myosin subfragment-1: a molecular motor, Science (New York, N.Y.), 261 (1993) 50-58.
[16] J.L. Fallon, D.B. Halling, S.L. Hamilton, F.A. Quiocho, Structure of calmodulin bound to the hydrophobic IQ domain of the cardiac $Ca_v1.2$ calcium channel, Structure (London, England : 1993), 13 (2005) 1881-1886.
[17] F. Van Petegem, F.C. Chatelain, D.L. Minor, Jr., Insights into voltage-gated calcium channel regulation from the structure of the $Ca_V1.2$ IQ domain-Ca^{2+}/calmodulin complex, Nat Struct Mol Biol, 12 (2005) 1108-1115.
[18] W.A. Catterall, Voltage-gated calcium channels, Cold Spring Harbor perspectives in biology, 3 (2011) a003947.
[19] A.C. Dolphin, Beta subunits of voltage-gated calcium channels, Journal of bioenergetics and biomembranes, 35 (2003) 599-620.
[20] A. Davies, J. Hendrich, A.T. Van Minh, J. Wratten, L. Douglas, A.C. Dolphin, Functional biology of the α2δ subunits of voltage-gated calcium channels, Trends Pharmacol Sci, 28 (2007) 220-228.
[21] H. Reuter, H. Porzig, Calcium channels. Diversity and complexity, Nature, 336 (1988) 113-114.
[22] H. Reuter, H. Porzig, S. Kokubun, B. Prod'hom, Calcium channels in the heart. Properties and modulation by dihydropyridine enantiomers, Ann N Y Acad Sci, 522 (1988) 16-24.
[23] R.W. Tsien, D. Lipscombe, D.V. Madison, K.R. Bley, A.P. Fox, Multiple types of neuronal calcium channels and their selective modulation, Trends in neurosciences, 11 (1988) 431-438.
[24] J.T. Littleton, B. Ganetzky, Ion channels and synaptic organization: analysis of the *Drosophila* genome, Neuron, 26 (2000) 35-43.
[25] V. Salvador-Recatala, R.M. Greenberg, Calcium channels of schistosomes: unresolved questions and unexpected answers, Wiley interdisciplinary reviews. Membrane transport and signaling, 1 (2012) 85-93.
[26] A.B. Kohn, J. Lea, J.M. Roberts-Misterly, P.A. Anderson, R.M. Greenberg, Structure of three high voltage-activated calcium channel α_1 subunits from *Schistosoma mansoni*, Parasitology, 123 (2001) 489-497.

[27] M. Berriman, B.J. Haas, P.T. LoVerde, R.A. Wilson, G.P. Dillon, G.C. Cerqueira, S.T. Mashiyama, B. Al-Lazikani, L.F. Andrade, P.D. Ashton, M.A. Aslett, D.C. Bartholomeu, G. Blandin, C.R. Caffrey, A. Coghlan, R. Coulson, T.A. Day, A. Delcher, R. DeMarco, A. Djikeng, T. Eyre, J.A. Gamble, E. Ghedin, Y. Gu, C. Hertz-Fowler, H. Hirai, Y. Hirai, R. Houston, A. Ivens, D.A. Johnston, D. Lacerda, C.D. Macedo, P. McVeigh, Z. Ning, G. Oliveira, J.P. Overington, J. Parkhill, M. Pertea, R.J. Pierce, A.V. Protasio, M.A. Quail, M.A. Rajandream, J. Rogers, M. Sajid, S.L. Salzberg, M. Stanke, A.R. Tivey, O. White, D.L. Williams, J. Wortman, W. Wu, M. Zamanian, A. Zerlotini, C.M. Fraser-Liggett, B.G. Barrell, N.M. El-Sayed, The genome of the blood fluke *Schistosoma mansoni*, Nature, 460 (2009) 352-358.
[28] B.Z. Peterson, C.D. DeMaria, J.P. Adelman, D.T. Yue, Calmodulin is the Ca^{2+} sensor for Ca^{2+}-dependent inactivation of L-type calcium channels, Neuron, 22 (1999) 549-558.
[29] N. Qin, R. Olcese, M. Bransby, T. Lin, L. Birnbaumer, Ca^{2+}-induced inhibition of the cardiac Ca^{2+} channel depends on calmodulin, Proc Natl Acad Sci U S A, 96 (1999) 2435-2438.
[30] W. Qin, S.G. Rane, E.K. Asem, Low extracellular Ca^{2+} activates a transient Cl^- current in chicken ovarian granulosa cells, Am J Physiol Cell Physiol, 279 (2000) C319-325.
[31] T. Budde, S. Meuth, H.C. Pape, Calcium-dependent inactivation of neuronal calcium channels, Nature reviews. Neuroscience, 3 (2002) 873-883.
[32] M.X. Mori, M.G. Erickson, D.T. Yue, Functional stoichiometry and local enrichment of calmodulin interacting with Ca^{2+} channels, Science, 304 (2004) 432-435.
[33] M.G. Erickson, B.A. Alseikhan, B.Z. Peterson, D.T. Yue, Preassociation of calmodulin with voltage-gated Ca^{2+} channels revealed by FRET in single living cells, Neuron, 31 (2001) 973-985.
[34] G.S. Pitt, R.D. Zuhlke, A. Hudmon, H. Schulman, H. Reuter, R.W. Tsien, Molecular basis of calmodulin tethering and Ca^{2+}-dependent inactivation of L-type Ca^{2+} channels, J Biol Chem, 276 (2001) 30794-30802.
[35] J. Utzinger, S.L. Becker, S. Knopp, J. Blum, A.L. Neumayr, J. Keiser, C.F. Hatz, Neglected tropical diseases: diagnosis, clinical management, treatment and control, Swiss medical weekly, 142 (2012) w13727.
[36] G.C. Coles, The effect of praziquantel on *Schistosoma mansoni*, Journal of helminthology, 53 (1979) 31-33.
[37] K.L. Blair, J.L. Bennett, R.A. Pax, Praziquantel: physiological evidence for its site(s) of action in magnesium-paralysed *Schistosoma mansoni*, Parasitology, 104 Pt 1 (1992) 59-66.
[38] J.D. Chan, M. Zarowiecki, J.S. Marchant, Ca^{2+} channels and praziquantel: a view from the free world, Parasitol Int, 62 (2013) 619-628.
[39] R.M. Greenberg, Are Ca^{2+} channels targets of praziquantel action?, International journal for parasitology, 35 (2005) 1-9.
[40] A.B. Kohn, P.A. Anderson, J.M. Roberts-Misterly, R.M. Greenberg, Schistosome calcium channel beta subunits. Unusual modulatory effects and potential role in the action of the antischistosomal drug praziquantel, J Biol Chem, 276 (2001) 36873-36876.
[41] A.B. Kohn, J.M. Roberts-Misterly, P.A. Anderson, R.M. Greenberg, Creation by mutagenesis of a mammalian Ca^{2+} channel beta subunit that confers praziquantel sensitivity to a mammalian Ca^{2+} channel, Int J Parasitol, 33 (2003) 1303-1308.
[42] E. Wolde Mussie, J. Vande Waa, R.A. Pax, R. Fetterer, J.L. Bennett, *Schistosoma mansoni*: calcium efflux and effects of calcium-free media on responses of the adult male musculature to praziquantel and other agents inducing contraction, Exp Parasitol, 53 (1982) 270-278.
[43] A.S. Taft, T.P. Yoshino, Cloning and functional characterization of two calmodulin genes during larval development in the parasitic flatworm *Schistosoma mansoni*, The Journal of parasitology, 97 (2011) 72-81.
[44] D.P. Thompson, G.Z. Chen, A.K. Sample, D.R. Semeyn, J.L. Bennett, Calmodulin: biochemical, physiological, and morphological effects on *Schistosoma mansoni*, The American Journal of Physiology, 251 (1986) R1051-1058.
[45] T. Katsumata, S. Kohno, K. Yamaguchi, K. Hara, Y. Aoki, Hatching of *Schistosoma mansoni* eggs is a Ca^{2+}/calmodulin-dependent process, Parasitology research, 76 (1989) 90-91.
[46] L.A. Kelley, M.J. Sternberg, Protein structure prediction on the Web: a case study using the Phyre server, Nature protocols, 4 (2009) 363-371.
[47] L.A. Kelley, S. Mezulis, C.M. Yates, M.N. Wass, M.J.E. Sternberg, The Phyre2 web portal for protein modeling, prediction and analysis, Nat. Protocols, 10 (2015) 845-858.
[48] E. Krieger, K. Joo, J. Lee, J. Lee, S. Raman, J. Thompson, M. Tyka, D. Baker, K. Karplus, Improving physical

realism, stereochemistry, and side-chain accuracy in homology modeling: Four approaches that performed well in CASP8, Proteins, 77 Suppl 9 (2009) 114-122.
[49] C.H. Yun, J. Bai, D.Y. Sun, D.F. Cui, W.R. Chang, D.C. Liang, Structure of potato calmodulin PCM6: the first report of the three-dimensional structure of a plant calmodulin, Acta Crystallogr D Biol Crystallogr, 60 (2004) 1214-1219.
[50] Y.S. Babu, C.E. Bugg, W.J. Cook, Structure of calmodulin refined at 2.2 Å resolution, Journal of Molecular Biology, 204 (1988) 191-204.
[51] J.L. Fallon, F.A. Quiocho, A closed compact structure of native Ca^{2+}-calmodulin, Structure, 11 (2003) 1303-1307.
[52] M.A. Schumacher, M. Crum, M.C. Miller, Crystal structures of apocalmodulin and an apocalmodulin/SK potassium channel gating domain complex, Structure, 12 (2004) 849-860.
[53] S.C. Lovell, I.W. Davis, W.B. Arendall, 3rd, P.I. de Bakker, J.M. Word, M.G. Prisant, J.S. Richardson, D.C. Richardson, Structure validation by Cα geometry: ϕ,ψ and Cβ deviation, Proteins, 50 (2003) 437-450.
[54] C.M. Thomas, D.J. Timson, FhCaBP2: a *Fasciola hepatica* calcium-binding protein with EF-hand and dynein light chain domains, Parasitology, 142 (2015) 1375-1386.
[55] M.M. Bradford, A rapid and sensitive method for the quantitation of microgram quantities of protein utilizing the principle of protein-dye binding, Analytical Biochemistry, 72 (1976) 248-254.
[56] E. Atcheson, E. Hamilton, S. Pathmanathan, B. Greer, P. Harriott, D.J. Timson, IQ-motif selectivity in human IQGAP2 and IQGAP3:binding of calmodulin and myosin essential light chain, Bioscience Reports, 31 (2011) 371-379.
[57] D.J. Timson, R.J. Reece, Functional analysis of disease-causing mutations in human galactokinase, European journal of biochemistry / FEBS, 270 (2003) 1767-1774.
[58] S. Banford, O. Drysdale, E.M. Hoey, A. Trudgett, D.J. Timson, FhCaBP3: A *Fasciola hepatica* calcium binding protein with EF-hand and dynein light chain domains, Biochimie, 95 (2013) 751-758.
[59] R. Orr, R. Kinkead, R. Newman, L. Anderson, E.M. Hoey, A. Trudgett, D.J. Timson, FhCaBP4: a *Fasciola hepatica* calcium-binding protein with EF-hand and dynein light chain domains, Parasitology research, 111 (2012) 1707-1713.
[60] S. Cheung, C.M. Thomas, D.J. Timson, FhCaBP1 (FH22): A *Fasciola hepatica* calcium-binding protein with EF-hand and dynein light chain domains, Exp Parasitol, 170 (2016) 109-115.
[61] C.M. Thomas, C.M. Fitzsimmons, D.W. Dunne, D.J. Timson, Comparative biochemical analysis of three members of the *Schistosoma mansoni* TAL family: Differences in ion and drug binding properties, Biochimie, 108 (2015) 40-47.
[62] J. Carson, C.M. Thomas, A. McGinty, G. Takata, D.J. Timson, The tegumental allergen-like proteins of *Schistosoma mansoni*: A biochemical study of SmTAL4-TAL13, Mol Biochem Parasitol, 221 (2018) 14-22.
[63] S. Datta, U.S. Annapure, D.J. Timson, Characterization of Cd36_03230p, a putative vanillin dehydrogenase from *Candida dubliniensis*, RSC Advances, 6 (2016) 99774-99780.
[64] A. Ortega, D. Amoros, J. Garcia de la Torre, Prediction of hydrodynamic and other solution properties of rigid proteins from atomic- and residue-level models, Biophys J, 101 (2011) 892-898.
[65] H.P. Erickson, Size and shape of protein molecules at the nanometer level determined by sedimentation, gel filtration, and electron microscopy, Biological procedures online, 11 (2009) 32-51.
[66] C.M. Thomas, D.J. Timson, Characterisation of calcium binding proteins from parasitic worms, Methods in Molecular Biology, In press (2018).
[67] T.C.t. Edrington, P.L. Yeagle, C.L. Gretzula, K. Boesze-Battaglia, Calcium-dependent association of calmodulin with the C-terminal domain of the tetraspanin protein peripherin/rds, Biochemistry, 46 (2007) 3862-3871.
[68] J.R. Lakowicz, Principles of Fluorescence Spectroscopy, Springer US, New York, 2006.
[69] G.M. Edelman, W.O. McClure, Fluorescent probes and the conformation of proteins, Accounts of Chemical Research, 1 (1968) 65-70.
[70] B.A. Seaton, J.F. Head, D.M. Engelman, F.M. Richards, Calcium-induced increase in the radius of gyration and maximum dimension of calmodulin measured by small-angle X-ray scattering, Biochemistry, 24 (1985) 6740-6743.
[71] M. Ikura, L.E. Kay, M. Krinks, A. Bax, Triple-resonance multidimensional NMR study of calmodulin complexed with the binding domain of skeletal muscle myosin light-chain kinase: indication of a

conformational change in the central helix, Biochemistry, 30 (1991) 5498-5504.
[72] G. Barbato, M. Ikura, L.E. Kay, R.W. Pastor, A. Bax, Backbone dynamics of calmodulin studied by ^{15}N relaxation using inverse detected two-dimensional NMR spectroscopy: the central helix is flexible, Biochemistry, 31 (1992) 5269-5278.
[73] M.A. Wilson, A.T. Brunger, The 1.0 Å crystal structure of Ca^{2+}-bound calmodulin: an analysis of disorder and implications for functionally relevant plasticity, Journal of Molecular Biology, 301 (2000) 1237-1256.
[74] Z. Grabarek, Structural basis for diversity of the EF-hand calcium-binding proteins, J Mol Biol, 359 (2006) 509-525.
[75] W.E. Meador, A.R. Means, F.A. Quiocho, Target enzyme recognition by calmodulin: 2.4 Å structure of a calmodulin-peptide complex, Science, 257 (1992) 1251-1255.
[76] S.H. Chao, Y. Suzuki, J.R. Zysk, W.Y. Cheung, Activation of calmodulin by various metal cations as a function of ionic radius, Mol Pharmacol, 26 (1984) 75-82.
[77] G. Richardt, G. Federolf, E. Habermann, Affinity of heavy metal ions to intracellular Ca^{2+}-binding proteins, Biochem Pharmacol, 35 (1986) 1331-1335.
[78] H. Ouyang, H.J. Vogel, Metal ion binding to calmodulin: NMR and fluorescence studies, Biometals : an international journal on the role of metal ions in biology, biochemistry, and medicine, 11 (1998) 213-222.
[79] T. Ozawa, K. Sasaki, Y. Umezawa, Metal ion selectivity for formation of the calmodulin-metal-target peptide ternary complex studied by surface plasmon resonance spectroscopy, Biochim Biophys Acta, 1434 (1999) 211-220.
[80] P. Kursula, V. Majava, A structural insight into lead neurotoxicity and calmodulin activation by heavy metals, Acta crystallographica. Section F, Structural biology and crystallization communications, 63 (2007) 653-656.
[81] F.T. Senguen, Z. Grabarek, X-ray structures of magnesium and manganese complexes with the N-terminal domain of calmodulin: insights into the mechanism and specificity of metal ion binding to an EF-hand, Biochemistry, 51 (2012) 6182-6194.
[82] D. Lafitte, A.J. Heck, T.J. Hill, K. Jumel, S.E. Harding, P.J. Derrick, Evidence of noncovalent dimerization of calmodulin, European journal of biochemistry / FEBS, 261 (1999) 337-344.
[83] J.B. Thoden, D.J. Timson, R.J. Reece, H.M. Holden, Molecular structure of human galactokinase: implications for type II galactosemia, Journal of Biological Chemistry, 280 (2005) 9662-9670.
[84] W. Tang, D.B. Halling, D.J. Black, P. Pate, J.Z. Zhang, S. Pedersen, R.A. Altschuld, S.L. Hamilton, Apocalmodulin and Ca^{2+} calmodulin-binding sites on the $Ca_{V1.2}$ channel, Biophys J, 85 (2003) 1538-1547.
[85] F. Findeisen, D.L. Minor, Jr., Structural basis for the differential effects of CaBP1 and calmodulin on $Ca_V1.2$ calcium-dependent inactivation, Structure, 18 (2010) 1617-1631.
[86] M. Ben-Johny, D.T. Yue, Calmodulin regulation (calmodulation) of voltage-gated calcium channels, The Journal of general physiology, 143 (2014) 679-692.
[87] E.Y. Kim, C.H. Rumpf, Y. Fujiwara, E.S. Cooley, F. Van Petegem, D.L. Minor, Jr., Structures of Ca_V2 Ca^{2+}/CaM-IQ domain complexes reveal binding modes that underlie calcium-dependent inactivation and facilitation, Structure, 16 (2008) 1455-1467.
[88] D.B. Halling, D.K. Georgiou, D.J. Black, G. Yang, J.L. Fallon, F.A. Quiocho, S.E. Pedersen, S.L. Hamilton, Determinants in Ca_V1 channels that regulate the Ca^{2+} sensitivity of bound calmodulin, J Biol Chem, 284 (2009) 20041-20051.
[89] D.R. Marshak, T.J. Lukas, D.M. Watterson, Drug-protein interactions: binding of chlorpromazine to calmodulin, calmodulin fragments, and related calcium binding proteins, Biochemistry, 24 (1985) 144-150.
[90] L. Massom, H. Lee, H.W. Jarrett, Trifluoperazine binding to porcine brain calmodulin and skeletal muscle troponin C, Biochemistry, 29 (1990) 671-681.
[91] M. Gnanasekar, A.M. Salunkhe, A.K. Mallia, Y.X. He, R. Kalyanasundaram, Praziquantel affects the regulatory myosin light chain of *Schistosoma mansoni*, Antimicrobial Agents and Chemotherapy, 53 (2009) 1054-1060.
[92] C.M. Fitzsimmons, F.M. Jones, A. Stearn, I.W. Chalmers, K.F. Hoffmann, J. Wawrzyniak, S. Wilson, N.B. Kabatereine, D.W. Dunne, The *Schistosoma mansoni* tegumental-allergen-like (TAL) protein family: influence of developmental expression on human IgE responses, PLoS neglected tropical diseases, 6 (2012) e1593.
[93] L.A. Ryan, E. Hoey, A. Trudgett, I. Fairweather, M. Fuchs, M.W. Robinson, E. Chambers, D.J. Timson, E. Ryan, T. Feltwell, A. Ivens, G. Bentley, D. Johnston, *Fasciola hepatica* expresses multiple α- and β-tubulin

isotypes, Molecular and biochemical parasitology, 159 (2008) 73-78.
[94] M.A. Fuchs, L.A. Ryan, E.L. Chambers, C.M. Moore, I. Fairweather, A. Trudgett, D.J. Timson, G.P. Brennan, E.M. Hoey, Differential expression of liver fluke β-tubulin isotypes at selected life cycle stages, Int J Parasitol, 43 (2013) 1133-1139.
[95] S.L. Russell, N.V. McFerran, E.M. Hoey, A. Trudgett, D.J. Timson, Characterisation of two calmodulin-like proteins from the liver fluke, *Fasciola hepatica*, Biological Chemistry, 388 (2007) 593-599.
[96] S.L. Russell, N.V. McFerran, C.M. Moore, Y. Tsang, P. Glass, E.M. Hoey, A. Trudgett, D.J. Timson, A novel calmodulin-like protein from the liver fluke, *Fasciola hepatica*, Biochimie, 94 (2012) 2398-2406.
[97] J. Zhou, J. Sun, Y. Huang, C. Zhou, P. Liang, M. Zheng, C. Liang, J. Xu, X. Li, X. Yu, Molecular identification, immunolocalization, and characterization of *Clonorchis sinensis* calmodulin, Parasitol Res, 112 (2013) 1709-1717.
[98] C.M. Moore, E.M. Hoey, A. Trudgett, D.J. Timson, A plasma membrane Ca^{2+}-ATPase (PMCA) from the liver fluke, *Fasciola hepatica*, International journal for parasitology, 42 (2012) 851-858.
[99] H. Tidow, P. Nissen, Structural diversity of calmodulin binding to its target sites, FEBS J., 280 (2013) 5551-5565.
[100] B. Weiss, W.C. Prozialeck, T.L. Wallace, Interaction of drugs with calmodulin. Biochemical, pharmacological and clinical implications, Biochemical pharmacology, 31 (1982) 2217-2226.
[101] R.V. Carsia, W.R. Moyle, D.J. Wolff, S. Malamed, Acute inhibition of corticosteroidogenesis by inhibitors of calmodulin action, Endocrinology, 111 (1982) 1456-1461.
[102] D.P. Giedroc, T.M. Keravis, J.V. Staros, N. Ling, J.N. Wells, D. Puett, Functional properties of covalent β-endorphin peptide/calmodulin complexes. Chlorpromazine binding and phosphodiesterase activation, Biochemistry, 24 (1985) 1203-1211.
[103] M. Vandonselaar, R.A. Hickie, J.W. Quail, L.T. Delbaere, Trifluoperazine-induced conformational change in Ca^{2+}-calmodulin, Nature structural biology, 1 (1994) 795-801.
[104] W.J. Cook, L.J. Walter, M.R. Walter, Drug binding by calmodulin: crystal structure of a calmodulin-trifluoperazine complex, Biochemistry, 33 (1994) 15259-15265.
[105] B.G. Vertessy, V. Harmat, Z. Bocskei, G. Naray-Szabo, F. Orosz, J. Ovadi, Simultaneous binding of drugs with different chemical structures to Ca^{2+}-calmodulin: crystallographic and spectroscopic studies, Biochemistry, 37 (1998) 15300-15310.
[106] E.M. McCammick, P. McVeigh, P. McCusker, D.J. Timson, R.M. Morphew, P.M. Brophy, N.J. Marks, A. Mousley, A.G. Maule, Calmodulin disruption impacts growth and motility in juvenile liver fluke, Parasit Vectors, 9 (2016) 46.
[107] D. Cioli, L. Pica-Mattoccia, Praziquantel, Parasitol Res, 90 Supp 1 (2003) S3-9.
[108] T. McLellan, Electrophoresis buffers for polyacrylamide gels at various pH, Analytical Biochemistry, 126 (1982) 94-99.
[109] K. Tamura, G. Stecher, D. Peterson, A. Filipski, S. Kumar, MEGA6: Molecular Evolutionary Genetics Analysis version 6.0, Mol Biol Evol, 30 (2013) 2725-2729.
[110] A.R. Rhoads, F. Friedberg, Sequence motifs for calmodulin recognition, FASEB journal : official publication of the Federation of American Societies for Experimental Biology, 11 (1997) 331-340.

“closed”

“collapsed”

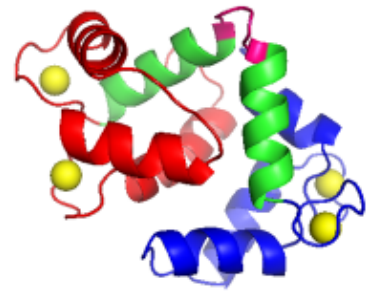

“open”

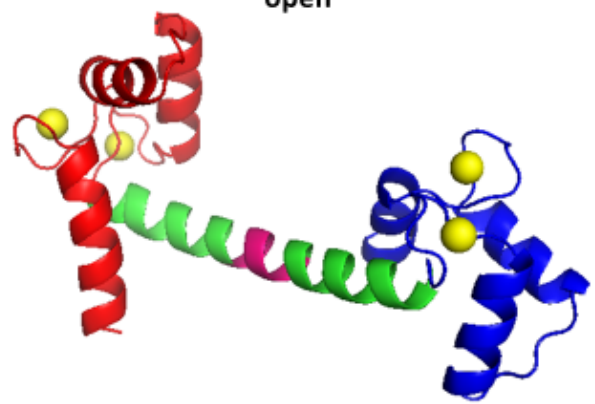

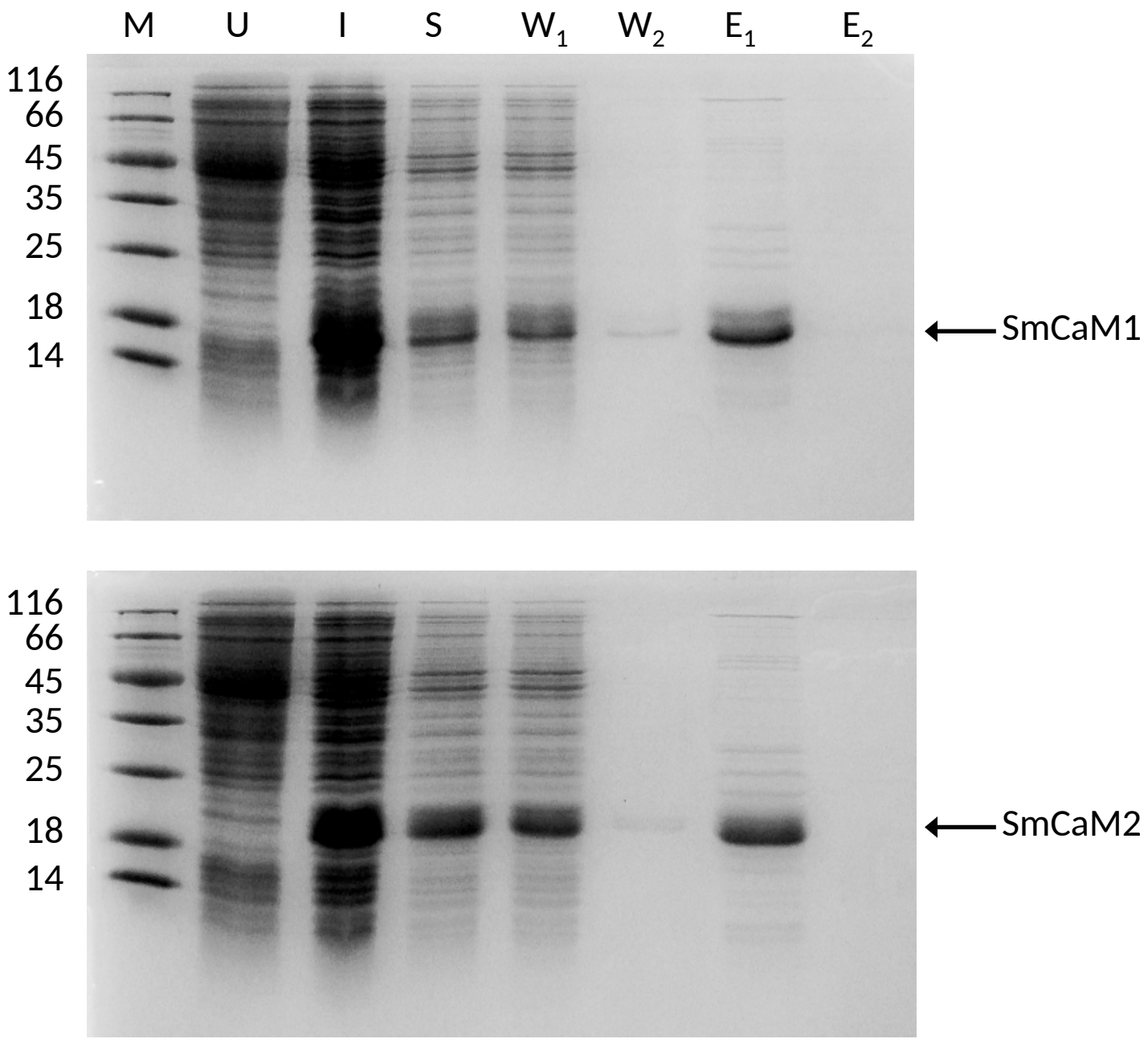
M
U
I
S
W1
W2
E1
E2
116
66
45
35
25
18
14
SmCaM1
116
66
45
35
25
18
14
SmCaM2

(a)

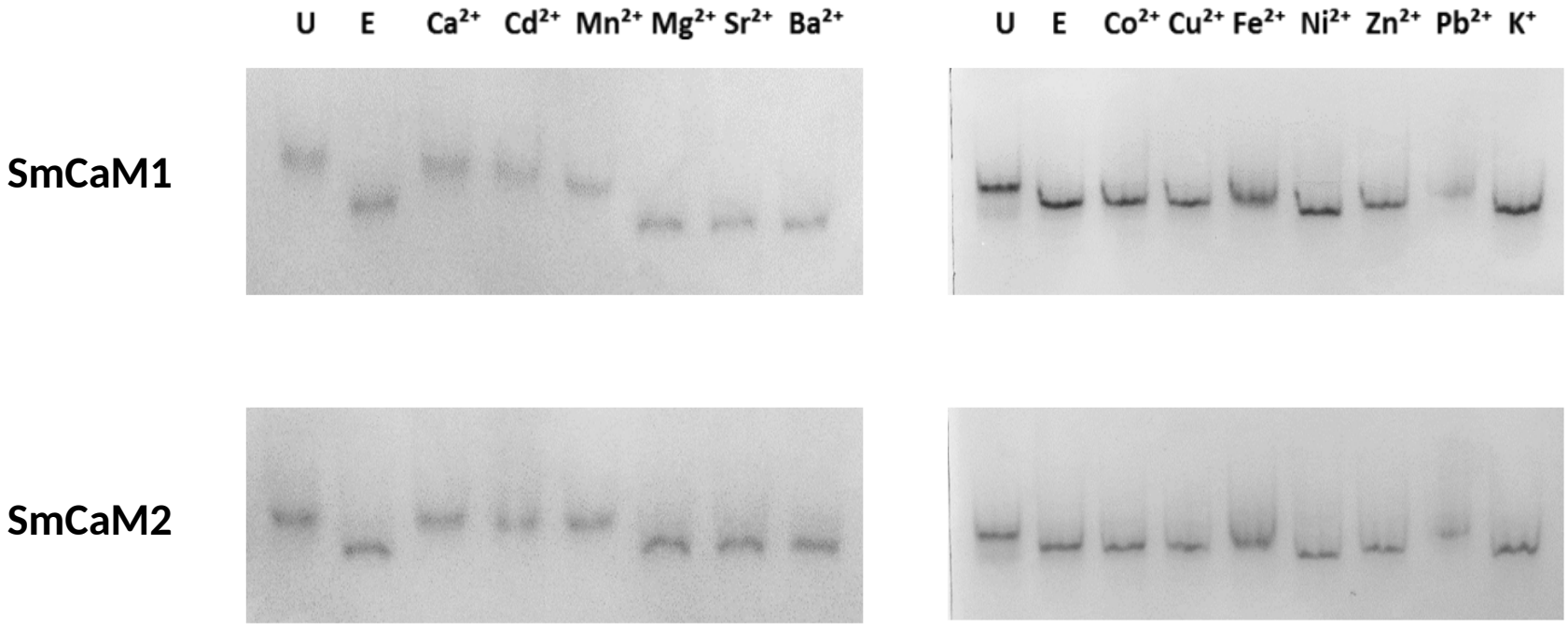
U E Ca2+ Cd2+ Mn2+ Mg2+ Sr2+ Ba2+
U E Co2+ Cu2+ Fe2+ Ni2+ Zn2+ Pb2+ K+
SmCaM1
SmCaM2

(b)

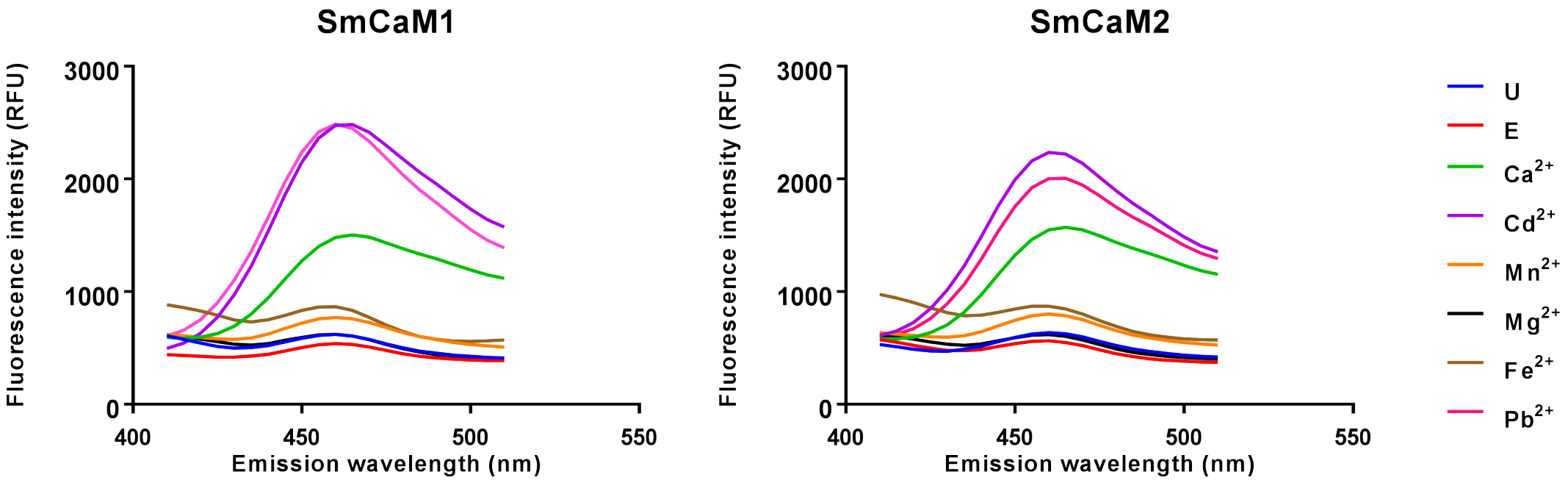
SmCaM1
SmCaM2
Fluorescence intensity (RFU)
3000
2000
1000
0
400
450
500
550
Emission wavelength (nm)
U
E
Ca2+
Cd2+
Mn2+
Mg2+
Fe2+
Pb2+

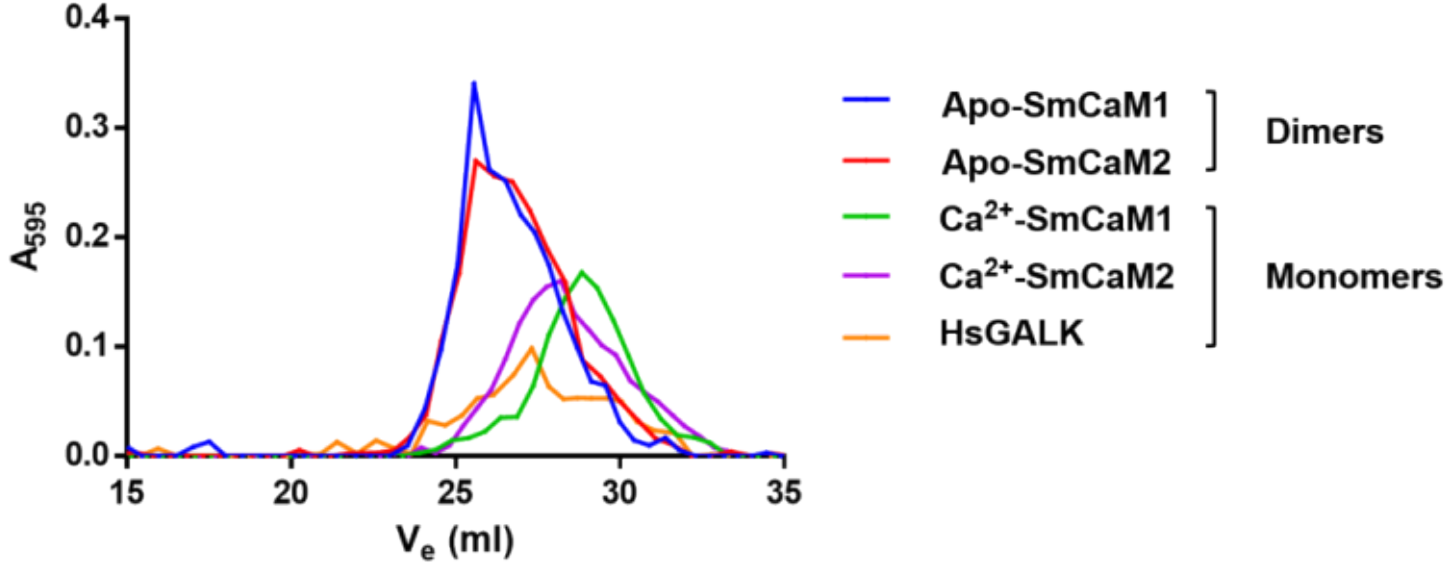
0.4
0.3
0.2
0.1
0.0
A595
15
20
25
30
35
Ve (ml)
Apo-SmCaM1
Apo-SmCaM2
Ca2+-SmCaM1
Ca2+-SmCaM2
HsGALK
Dimers
Monomers

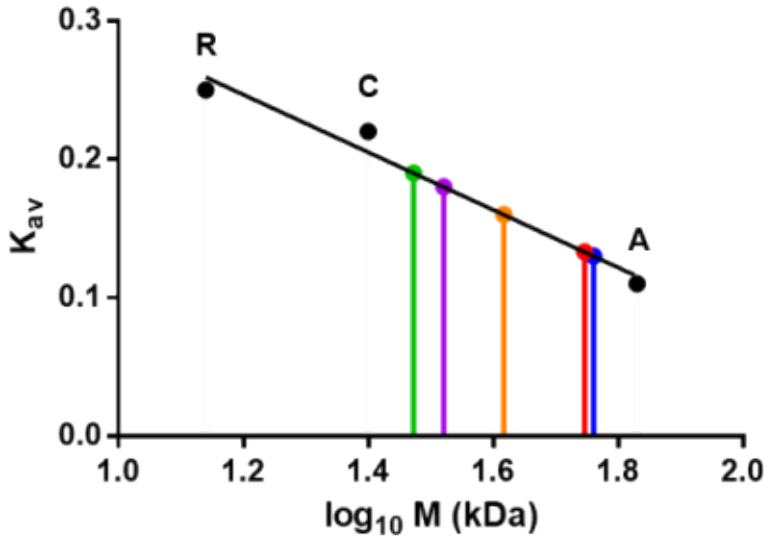
0.3
0.2
0.1
0.0
Kav
R
C
A
1.0
1.2
1.4
1.6
1.8
2.0
log10 M (kDa)

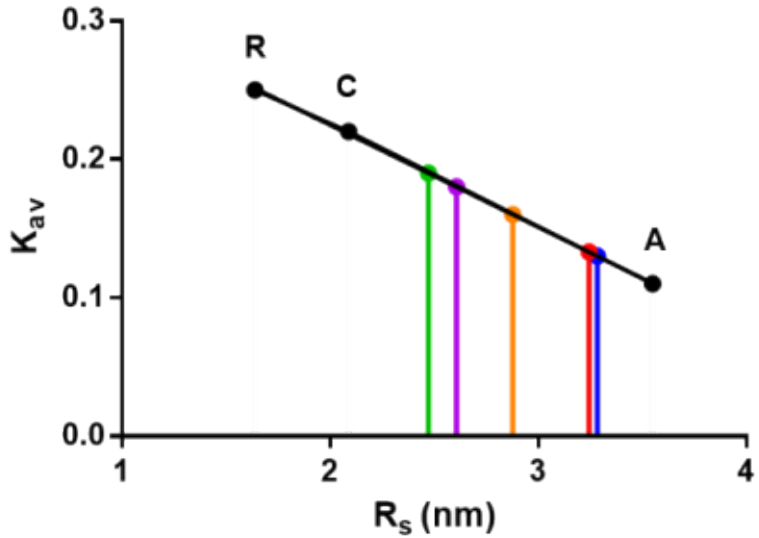
0.3
0.2
0.1
0.0
Kav
R
C
A
1
2
3
4
Rs (nm)

```
 IQ consensus:  --------IQxxxRGxxxR----
                  **  *    **  *
SmIQ1  (1528):  GKFYATFLIQNWFREWQKRKMIQKDTR
SmIQ2  (1580):  SSDLTGDEIQRR-RGVDKRDTSGGIFG
SmIQ3  (1923):  GKFYATFLIQEWFRRWKQKKAEEQKAL
Cav1.1 (1521):  GFKYATFLIQEHFRKFMKRQEEYYGYR
Cav1.2 (1613):  GKFYATFLIQEYFRKFKKRKEQGLVGK
Cav1.3 (1604):  GKFYATFLIQDYFRKFKKRKEQGLVGK
Cav1.4 (1581):  GKFYATFLIQDYFRKFRRRKEKGLLGN

SmIQ4  (1573):  GKIYAGLLIYENWQMNKSTGNKKNLHQ
Cav2.1 (1954):  GKIYAAMMIMEYYRQSKAKKLQAMREE
Cav2.2 (1954):  GKVYAALMIFDFYKQNKTTRDQMQQAP
Cav2.3 (1866):  GKIYAAMMIMDYYKQSKVKKQRQQLEE
```

(a)

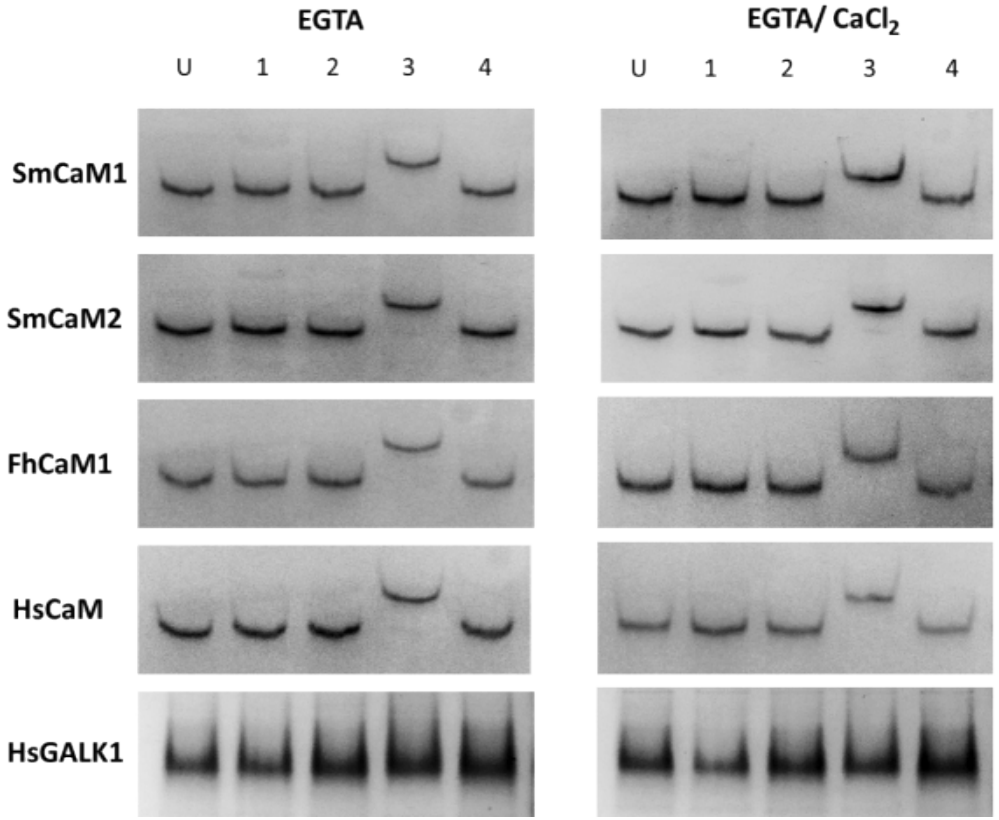
EGTA
EGTA/ CaCl2
U 1 2 3 4
U 1 2 3 4
SmCaM1
SmCaM2
FhCaM1
HsCaM
HsGALK1

(b)

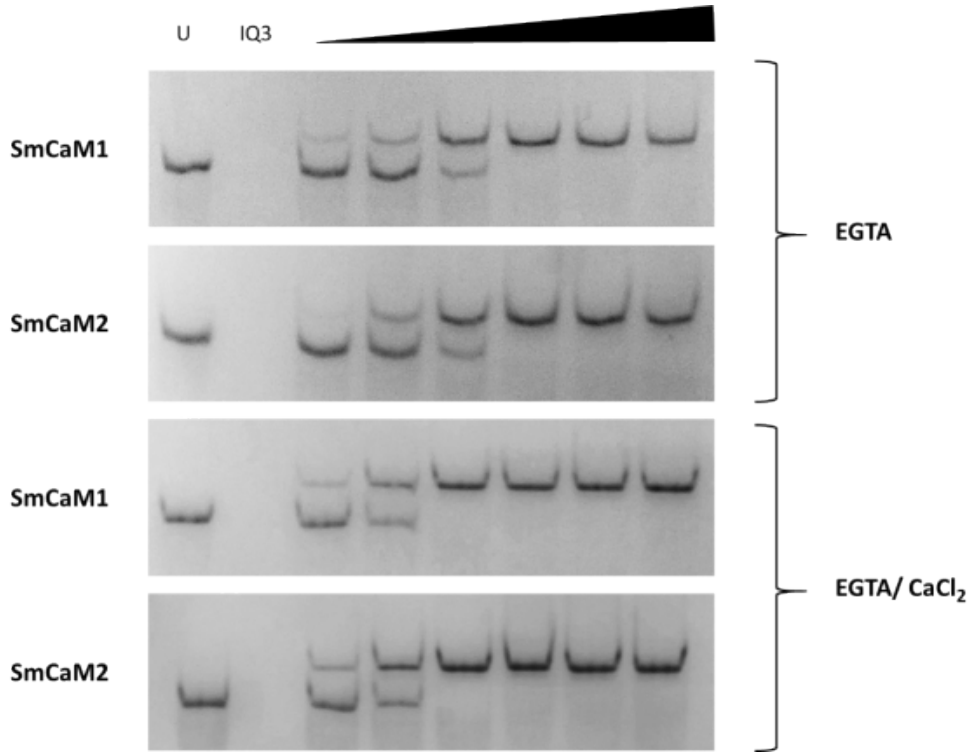
U
IQ3
SmCaM1
SmCaM2
SmCaM1
SmCaM2
EGTA
EGTA/ CaCl2

SmCaM1 (no calcium)

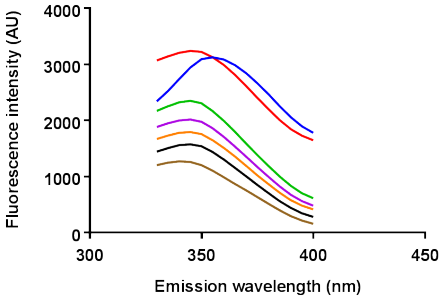

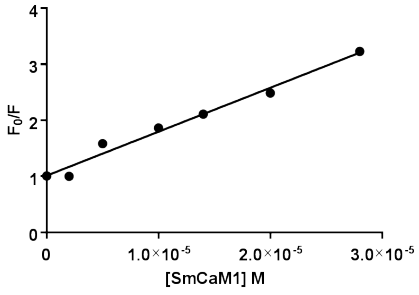

SmCaM2 (no calcium)

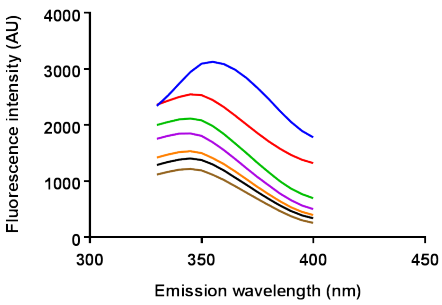

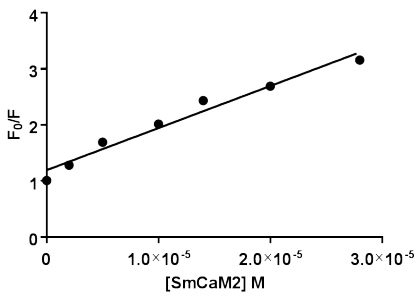

SmCaM1 (calcium)

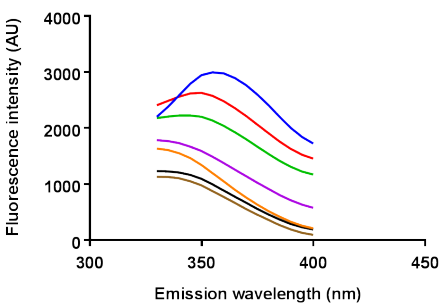

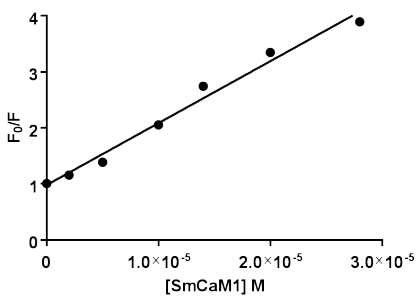

SmCaM2 (calcium)

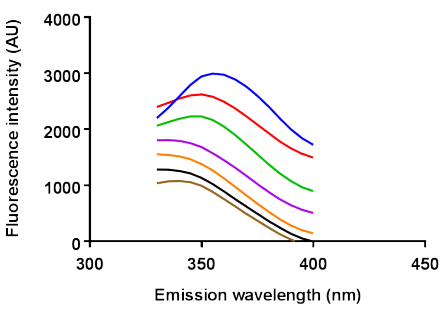

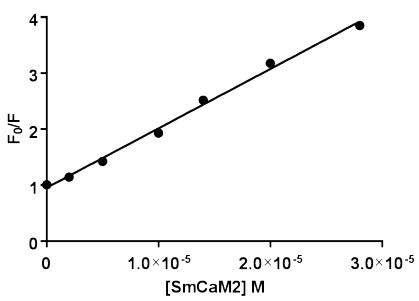

(a)

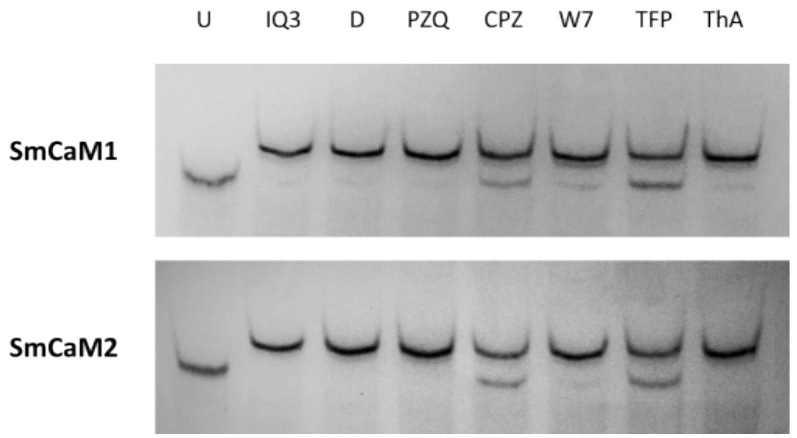
U
IQ3
D
PZQ
CPZ
W7
TFP
ThA
SmCaM1
SmCaM2

(b)

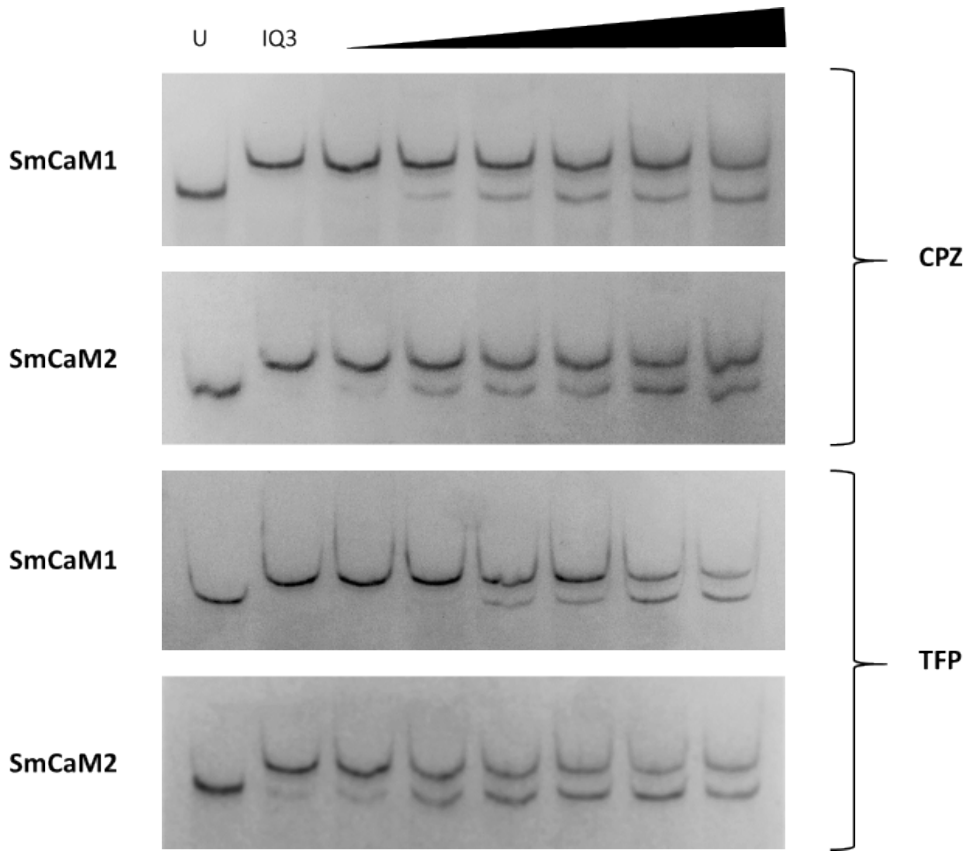
U
IQ3
SmCaM1
SmCaM2
CPZ
SmCaM1
SmCaM2
TFP

Calmodulins from *Schistosoma mansoni*: biochemical analysis and interaction with IQ-motifs from voltage-gated calcium channels

Charlotte M. Thomas and David J. Timson

Neither of us have any conflicts of interest.

Calmodulins from *Schistosoma mansoni*: biochemical analysis and interaction with IQ-motifs from voltage-gated calcium channels

Charlotte M. Thomas and David J. Timson

Both of us have seen and approved the final version of the manuscript being submitted. We warrant that the article is our original work, has not received prior publication and is not under consideration for publication elsewhere.

Neither of us have any conflicts of interest.